The postmitotic nature of neurons may underlie the age-dependent NIA of mutant DRPLA proteins starting on P4. Although further analysis is required, we speculate that regional differences in the synthesis, processing and subcellular localizations of mutant DRPLA proteins (33–35) play key roles in the region-specific distribution of NIA.

Neuronal dysfunction without neuronal loss is essential in DRPLA pathogenesis

Intriguingly, we have not observed any neuronal loss in the brains of the Q129 mice despite the progressive brain atrophy and severe neurological phenotypes. Indeed, the electrophysiological analyses demonstrated age-dependent and region-specific synaptic dysfunction along with disease progression. We demonstrated presynaptic dysfunction (altered PPRs) in PCs and pallidal neurons, and postsynaptic dysfunction (shrinkage of distal dendrites of PCs and decreased currents through AMPA and $GABA_A$ receptors in CA1 neurons). These observations strongly argue for the concept of 'neuronal dysfunction without neuronal death'. Our recent morphometric studies demonstrated marked reductions in the number and size of spines, further supporting synaptic dysfunction (14).

The concept of neuronal dysfunction without neuronal death is apparently contradictory to the neuropathological finding that neuronal loss confined to DRPL systems is the hallmark of DRPLA. As discussed above, neurological phenotypes presumably reflect neuronal dysfunction as a result of NIA, and neuronal loss may well be the latest event observed in advanced stages. Supporting this concept, juvenile-onset DRPLA patients initially do not show markedly atrophic changes in the cerebellum in magnetic resonance imaging, in contrast to markedly atrophic changes observed in late-adult-onset DRPLA patients (36).

Transcriptional dysregulations and neuronal dysfunction

In this study, we have identified genes that are down-regulated in an age-dependent manner, including those coding for neuropeptides, transcriptional factors and signaling molecules. Because of the functional relevance and strong down-regulation even at 4 weeks of age, kalirin is of particular interest, which is a multifunctional Rho guanine nucleotide exchange factor, also known as the huntingtin-associated protein interacting protein (37). The age-dependent decrease in the expression level of kalirin in the Q129 mouse brain was further confirmed by western blot analysis (Supplementary Material, Fig. S1). It has been demonstrated that the down-regulation of kalirin results in reduced linear spine density and the elimination of presynaptic endings in CA1 hippocampal neurons (38). Because the reduction in spine density is the most striking change in our morphometric analysis of Q129 mice (14), the down-regulation of kalirin might be directly involved in synaptic dysfunction. Although the functional relevance was not discussed, the down-regulation of kalirin was also observed in R6/2 mice (39; described as the expression sequence tag AA673405).

In the category of neuropeptides, arginine vasopressin showed the most striking down-regulation, which is consistent with the phenotype of central diabetes insipidus. Although clinically apparent endocrinological dysfunction has not been described in DRPLA patients, detailed investigations should be carried out on DRPLA patients, particularly on those with juvenile-onset DRPLA and highly expanded CAG repeats. Given the behavioral abnormalities observed in mice with their neuropeptides knocked out, including somatostatin (MGI:98326, impairment in motor learning) and neuropeptide Y (MGI:97374, seizure), the down-regulation of these neuropeptides may also contribute in part to the behavioral abnormalities of the Q129 mice. Dbp (MGI:2183196), Fos (MGI:95574) or excitatory amino acid transporter 2 (Slc1a2, MGI:101931) knock-out mice show seizures, suggesting that the down-regulation of these genes may also contribute to the neurological phenotypes of Q129 mice.

As shown in Figure 6, 46% of down-regulated and 61% of strongly down-regulated genes (fold change < -1.5) have CRE sites. These observations support our previous finding that CREB-dependent transcriptional activation is strongly suppressed by expanded polyQ stretches in cellular models (11,12,40). A role for CREB-mediated signaling in neurodegeneration has been provided by Mantamadiotis *et al.* (41), as determined using conditional CREB knock-out mice. They described that mice lacking both CREB and cAMP response element modulator protein (CREM) in the postnatal forebrain showed progressive neurodegeneration of the striatum and hippocampus after 1.5 months, and a neurological phenotype after 6 months, supporting the hypothesis that disruption of CREB-dependent transcription plays an essential role in neurodegeneration in polyQ diseases through transcriptional dysregulations. Although we focused on CREB-dependent transcription, it has recently been reported that expanded polyQ stretches disrupt the structures of $TAF_{II}D$ and $TAF_{II}F$ of the basal transcriptional apparatus (42). Thus, the down-regulation of genes may involve multiple mechanisms in addition to the down-regulation of CREB target genes; further investigations on the mechanisms underlying transcriptional dysregulations caused by expanded polyQ stretches should be carried out.

We should emphasize the concept of neuronal dysfunction without neuronal death as the essential pathophysiologic mechanism underlying polyQ diseases, which are associated with transcriptional dysregulations. This concept is further supported by a previous study that demonstrated the reversible recovery of phenotypic presentations in an HD mouse model after the shut-off of the expression of truncated mutant *huntingtin* (43). A recent report of deficits in experience-dependent cortical plasticity in presymptomatic HD mice (44) further strengthens this concept. This concept strongly emphasizes a wider time interval for therapeutic interventions. Because our Q129 mice closely replicate pathophysiologic processes in the human brain, as supported by the insertion of a single copy gene with its own promoter, the Q129 mice should be an ideal model for exploring possibilities for therapeutic interventions aimed at polyQ diseases.

MATERIALS AND METHODS

Generation and background of Q129 mice

Q76 transgenic mice were previously established in N1 progenies (Drm21 line) with agouti coat color that were generated from a CCE ES clone (13). Q76 mice were backcrossed to C57BL/6J, and the EF121 mosaic mouse (Q129-76) that

bred the Q129 mice (see Results) was found in the N3 generation. The EF121 mosaic mouse was also crossed with C57BL/6J females. Q129 mice used for analyses of phenotypes and expression profiling were from the N4 or N5 generation, and those used for electrophysiological analysis were from N6 or later generations. Q129 mice were established by *in vitro* fertilization using male transgenic mice at 12 weeks of age.

Brain slice preparation

Q129 transgenic mice or their age-matched non-TG littermates at either 1 to 2 weeks, 4–5 weeks or 12–15 weeks of age were decapitated under ether anesthesia. Their brains were isolated and were placed in ice-cold artificial cerebrospinal fluid (ACSF) containing NaCl (124 mM), KCl (3 mM), NaH_2PO_4 (1 mM), $MgCl_2$ (1.2 mM), $CaCl_2$ (2.4 mM) and glucose (10 mM), buffered at pH 7.4 with $NaHCO_3$ (26 mM) and saturated with 95% O_2 and 5% CO_2. The cerebellar and pallidal slices were cut parasagittally (250 μm thick) as previously described (45,46). For the preparation of hippocampal slices (250 and 400 μm thick; used for whole-cell and field recording, respectively), hippocampal formations were dissected free and cut with a tissue slicer.

Field recording

Hippocampal fEPSPs were recorded using glass electrodes (filled with ACSF) placed in the stratum radiatum of area CA1. Field EPSPs were evoked by stimulating the Schaffer collateral/commissural pathway with short current pulses (50 μs duration; 0.033 Hz) using a Teflon-coated bipolar tungsten electrode (Microprobe, Potomac, MD). LTP was induced by either one or four trains of tetanic stimulation (100 pulses/100 Hz; intertrain interval, 2 s) and monitored for 4–5 h after the tetanic stimulation to detect late-phase LTP.

Whole-cell recording

Whole-cell patch-clamp recording was made by infrared differential contrast visualization. For voltage-clamp recording in the GP and hippocampus, patch pipettes (4–6 MΩ) containing Cs-methanesulfonate (124 mM), KCl (11 mM), $MgCl_2$ (2 mM), HEPES (10 mM), Na_2-ATP (4 mM), GTP (0.3 mM), spermine (0.1 mM), QX-314 (5 mM) and 0.5% biocytin (adjusted to 280 mOsm and pH 7.3 with CsOH) were used. For recording from neurons in cerebellar nuclei, patch pipettes (4–6 MΩ) containing CsCl (30 mM), CsOH (110 mM), EGTA (1.0 mM), HEPES (10 mM), $MgCl_2$ (4.6 mM), $CaCl_2$ (0.1 mM), Na_2-ATP (4 mM) and Na_2-GTP (0.4 mM) (pH 7.3, adjusted with D-gluconate, 280 Osm, $E_{Cl} = -30$ mV) were used. For recording from PCs in the cerebellar cortex, patch pipettes (3–5 MΩ) containing CsCl (60 mM), Cs D-gluconate (10 mM), TEA-Cl (20 mM), BAPTA (20 mM), HEPES (30 mM), $MgCl_2$ (4 mM), Na_2-ATP (4 mM) and Na_2-GTP (0.4 mM) (pH 7.3, adjusted with CsOH, 280 Osm) were used.

Bicuculline methiodide (20 μM) was added to isolate glutamatergic currents. To isolate $GABA_A$ receptor-mediated currents, the NMDA receptor antagonist D(−)-2-amino-5-phosphonopentanoic acid (D-AP5, 25 μM) and the AMPA receptor antagonist 6-cyano-7-nitroquinoxaline-2,3-dione (CNQX, 10 μM) were applied to ACSF.

Immunohistochemical analysis

Q129, Q76 and non-TG littermates were anesthetized in ether and perfused with phosphate-buffered saline followed by 4% paraformaldehyde. The brains were removed and immersed in the same fixative for 16 h. Paraffin-embedded, 4-μm-thick sections were prepared and subjected to immunostaining with a rabbit polyclonal antibody against ubiquitin at 1:3200 dilution (Dako, Tokyo, Japan), the mouse monoclonal antibody 1C2 at 1:16 000 dilution (Chemicon, Temecula, CA) and goat polyclonal antibody APG840 at 1:2000 dilution as described previously (10).

RT–PCR analysis

Total RNAs were extracted from the brains (whole cerebrum and cerebellum). To avoid contamination with genomic DNA, total RNAs were extracted twice using ISOGEN (Nippon Gene, Tokyo, Japan) and converted into cDNA by priming with random hexamers using an Advantage RT-for-PCR Kit (Clontech, Mountain View, CA). PCR was performed in a 50 μl mixture containing 2.5 U AmpliTaq DNA polymerase (Applied Biosystems, Foster City, CA), 10 mM Tris–HCl (pH 8.3), 50 mM KCl, 1.5 mM $MgCl_2$, 200 μM dNTP and 5 pmol of each primer with an antisense primer labeled with FAM (5′-CTGCCCTGAGACCCCTCAA C-3′, 5′-FAM-TGGGATGGGAGAGAAGGCTG-3′). After an initial denaturation at 96°C for 2 min, PCR was performed for 30 cycles consisting of denaturation at 96°C for 45 s, annealing at 60°C for 1 min and extension at 72°C for 1 min, followed by a final extension at 72°C for 10 min. PCR products were quantified by determining the area of the chromatogram using an ABI 310 DNA sequencer and Genescan version 2.1 software (Applied Biosystems).

Western blot analysis

Brain samples from age-matched Q129, Q76 and non-TG littermates at 4, 8 and 12 weeks of age were prepared. From AT-FL-26Q-84 and AT-FL-65Q-150 mice (20), samples were obtained at 7.5 months of age; these mice were transgenic, expressing full-length DRPLA cDNAs encoding 26 and 65 CAG repeats, respectively. Sample preparation and western blot analysis were performed as described previously (17,20). Total homogenates, 20 μg per lane, and nuclear extracts, 30 and 35 μg per lane, were subjected to western blot analysis using the rabbit polyclonal antibody C580 (17), polyclonal antibody AP142 (18) and 1C2 (Chemicon), respectively.

Expression profiling analysis

Total RNAs were extracted similar to those for the RT–PCR analysis. Brain polyA(+) RNAs were prepared using an Oligotex-dT30⟨Super⟩mRNA Purification Kit (Takara, Otsu, Japan) and subjected to hybridization using Mu11KsubA and B oligonucleotide arrays (GeneChip) according to the

manufacturer's instructions (Affymetrix). Statistical analyses were performed by error-weighted ANOVA using the Rosetta Resolver gene expression data analysis system (Rosetta Biosoftware, Seattle, WA). For determining the number of dysregulated genes at 4 or 12 weeks of age, one-way ANOVA was first applied using intensity data (Time Slice). For post hoc analysis, the dysregulated genes, each of which showed both a significant difference in ratio data and an absolute fold change ≥ 1.5, were selected using the Rosetta Resolver (Ratio Experiment). For identifying the genes showing age-dependent changes, two-way ANOVA (variables: animal and time) was first applied. For post hoc analysis, genes showing a significant difference in ratio data at 12 weeks of age were selected using the Ratio Experiment. A P-value of <0.05 was considered to indicate a statistically significant difference.

SUPPLEMENTARY MATERIAL

Supplementary Material is available at *HMG* online.

ACKNOWLEDGEMENTS

We thank Satoshi Naruse, Shuichi Igarashi, Mutsuo Oyake, Hidetoshi Date, Yi Jin, Hitoshi Ichikawa, Misao Ohki, Michitoshi Watanabe, Michihiro Igarashi and Minesuke Yokoyama for helpful discussions, and Yoshitaka Yamamoto, Yoshitaka Maeda and Nobuyoshi Fujisawa for the management of laboratory animal facilities.

Conflict of Interest statement. None declared.

FUNDING

KAKENHI (Grant-in-Aid for Scientific Research) on Priority Areas (Applied Genomics and Advanced Brain Science Project), the 21st Century COE Program, Center for Integrated Brain Medical Science and Scientific Research (A) from the Ministry of Education, Culture, Sports, Science and Technology, Japan; a grant for Research for the Future Program from the Japan Society for the Promotion of Science; a grant from the Research Committee for Ataxic Diseases, the Ministry of Health, Labour and Welfare, Japan; a grant for Surveys and Research on Specific Diseases, the Ministry of Health, Labour and Welfare, Japan; the Takeda Science Foundation; the Tsubaki Memorial Neuroscience Research Foundation; and the Uehara Memorial Foundation. Funding to pay the Open Access publication charges for this article was provided by KAKENHI (Grant-in-Aid for Scientific Research) on Priority Areas (Applied Genomics).

REFERENCES

1. Naito, H. and Oyanagi, S. (1982) Familial myoclonus epilepsy and choreoathetosis: hereditary dentatorubral–pallidoluysian atrophy. *Neurology*, **32**, 798–807.
2. Takahashi, H., Ohama, E., Naito, H., Takeda, S., Nakashima, S., Makifuchi, T. and Ikuta, F. (1988) Hereditary dentatorubral–pallidoluysian atrophy: clinical and pathologic variants in a family. *Neurology*, **38**, 1065–1070.
3. Li, S.H., McInnis, M.G., Margolis, R.L., Antonarakis, S.E. and Ross, C.A. (1993) Novel triplet repeat containing genes in human brain: cloning, expression, and length polymorphisms. *Genomics*, **16**, 572–579.
4. Koide, R., Ikeuchi, T., Onodera, O., Tanaka, H., Igarashi, S., Endo, K., Takahashi, H., Kondo, R., Ishikawa, A., Hayashi, T. *et al.* (1994) Unstable expansion of CAG repeat in hereditary dentatorubral–pallidoluysian atrophy (DRPLA). *Nat. Genet.*, **6**, 9–13.
5. Nagafuchi, S., Yanagisawa, H., Sato, K., Shirayama, T., Ohsaki, E., Bundo, M., Takeda, T., Tadokoro, K., Kondo, I., Murayama, N. *et al.* (1994) Dentatorubral and pallidoluysian atrophy expansion of an unstable CAG trinucleotide on chromosome 12p. *Nat. Genet.*, **6**, 14–18.
6. Gatchel, J.R. and Zoghbi, H.Y. (2005) Diseases of unstable repeat expansion: mechanisms and common principles. *Nat. Rev. Genet.*, **6**, 743–755.
7. Davies, S.W., Turmaine, M., Cozens, B.A., DiFiglia, M., Sharp, A.H., Ross, C.A., Scherzinger, E., Wanker, E.E., Mangiarini, L. and Bates, G.P. (1997) Formation of neuronal intranuclear inclusions underlies the neurological dysfunction in mice transgenic for the HD mutation. *Cell*, **90**, 537–548.
8. Paulson, H.L., Perez, M.K., Trottier, Y., Trojanowski, J.Q., Subramony, S.H., Das, S.S., Vig, P., Mandel, J.L., Fischbeck, K.H. and Pittman, R.N. (1997) Intranuclear inclusions of expanded polyglutamine protein in spinocerebellar ataxia type 3. *Neuron*, **19**, 333–344.
9. Igarashi, S., Koide, R., Shimohata, T., Yamada, M., Hayashi, Y., Takano, H., Date, H., Oyake, M., Sato, T., Sato, A. *et al.* (1998) Suppression of aggregate formation and apoptosis by transglutaminase inhibitors in cells expressing truncated DRPLA protein with an expanded polyglutamine stretch. *Nat. Genet.*, **18**, 111–117.
10. Yamada, M., Wood, J.D., Shimohata, T., Hayashi, S., Tsuji, S., Ross, C.A. and Takahashi, H. (2001) Widespread occurrence of intranuclear atrophin-1 accumulation in the central nervous system neurons of patients with dentatorubral–pallidoluysian atrophy. *Ann. Neurol.*, **49**, 14–23.
11. Shimohata, T., Nakajima, T., Yamada, M., Uchida, C., Onodera, O., Naruse, S., Kimura, T., Koide, R., Nozaki, K., Sano, Y. *et al.* (2000) Expanded polyglutamine stretches interact with $TAF_{II}130$, interfering with CREB-dependent transcription. *Nat. Genet.*, **26**, 29–36.
12. Nucifora, F.C. Jr., Sasaki, M., Peters, M.F., Huang, H., Cooper, J.K., Yamada, M., Takahashi, H., Tsuji, S., Troncoso, J., Dawson, V.L. *et al.* (2001) Interference by huntingtin and atrophin-1 with CBP-mediated transcription leading to cellular toxicity. *Science*, **291**, 2423–2428.
13. Sato, T., Oyake, M., Nakamura, K., Nakao, K., Fukusima, Y., Onodera, O., Igarashi, S., Takano, H., Kikugawa, K., Ishida, Y. *et al.* (1999) Transgenic mice harboring a full-length human mutant *DRPLA* gene exhibit age-dependent intergenerational and somatic instabilities of CAG repeats comparable with those in DRPLA patients. *Hum. Mol. Genet.*, **8**, 99–106.
14. Sakai, K., Yamada, M., Sato, T., Yamada, M., Tsuji, S. and Takahashi, H. (2006) Neuronal atrophy and synaptic alteration in a mouse model of dentatorubral–pallidoluysian atrophy. *Brain*, **129**, 2353–2362.
15. Ikeuchi, T., Koide, R., Tanaka, H., Onodera, O., Igarashi, S., Takahashi, H., Kondo, R., Ishikawa, A., Tomoda, A., Miike, T. *et al.* (1995) Dentatorubral–pallidoluysian atrophy: clinical features are closely related to unstable expansions of trinucleotide (CAG) repeat. *Ann. Neurol.*, **37**, 769–775.
16. Llano, I., Marty, A., Armstrong, C.M. and Konnerth, A. (1991) Synaptic- and agonist-induced excitatory currents of Purkinje cells in rat cerebellar slices. *J. Physiol.*, **434**, 183–213.
17. Yazawa, I., Nukina, N., Hashida, H., Goto, J., Yamada, M. and Kanazawa, I. (1995) Abnormal gene product identified in hereditary dentatorubral–pallidoluysian atrophy (DRPLA) brain. *Nat. Genet.*, **10**, 99–103.
18. Wood, J.D., Yuan, J., Margolis, R.L., Colomer, V., Duan, K., Kushi, J., Kaminsky, Z., Kleiderlein, J.J. Jr., Sharp, A.H. and Ross, C.A. (1998) Atrophin-1, the *DRPLA* gene product, interacts with two families of WW domain-containing proteins. *Mol. Cell. Neurosci.*, **11**, 149–160.
19. Watase, K., Weeber, E.J., Xu, B., Antalffy, B., Yuva-Paylor, L., Hashimoto, K., Kano, M., Atkinson, R., Sun, Y., Armstrong, D.L. *et al.* (2002) A long CAG repeat in the mouse *Sca1* locus replicates SCA1 features and reveals the impact of protein solubility on selective neurodegeneration. *Neuron*, **34**, 905–919.
20. Schilling, G., Wood, J.D., Duan, K., Slunt, H.H., Gonzales, V., Yamada, M., Cooper, J.K., Margolis, R.L., Jenkins, N.A., Copeland, N.G. *et al.* (1999) Nuclear accumulation of truncated atrophin-1 fragments in a transgenic mouse model of DRPLA. *Neuron*, **24**, 275–286.

21. Mayr, B. and Montminy, M. (2001) Transcriptional regulation by the phosphorylation-dependent factor CREB. *Nat. Rev. Mol. Cell Biol.*, **2**, 599–609.
22. Zhang, X., Odom, D.T., Koo, S.H., Conkright, M.D., Canettieri, G., Best, J., Chen, H., Jenner, R., Herbolsheimer, E., Jacobsen, E. *et al.* (2005) Genome-wide analysis of cAMP-response element binding protein occupancy, phosphorylation, and target gene activation in human tissues. *Proc. Natl Acad. Sci. USA*, **102**, 4459–4464.
23. Myers, R.H., MacDonald, M.E., Koroshetz, W.J., Duyao, M.P., Ambrose, C.M., Taylor, S.A.M., Barnes, G., Srinidhi, J., Lin, C.S., Whaley, W.L. *et al.* (1993) *De novo* expansion of a $(CAG)_n$ repeat in sporadic Huntington's disease. *Nat. Genet.*, **5**, 168–173.
24. Goldberg, Y.P., Kremer, B., Andrew, S.E., Theilmann, J., Graham, R.K., Squitieri, F., Telenius, H., Adam, S., Sajoo, A., Starr, E. *et al.* (1993) Molecular analysis of new mutations for Huntington's disease: intermediate alleles and sex of origin effects. *Nat. Genet.*, **5**, 174–179.
25. Stevanin, G., Giunti, P., David, G., Belal, S., Dürr, A., Ruberg, M., Wood, N. and Brice, A. (1998) *De novo* expansion of intermediate alleles in spinocerebellar ataxia 7. *Hum. Mol. Genet.*, **7**, 1809–1813.
26. Koide, R., Kobayashi, S., Shimohata, T., Ikeuchi, T., Maruyama, M., Saito, M., Yamada, M., Takahashi, H. and Tsuji, S. (1999) A neurological disease caused by an expanded CAG trinucleotide repeat in the TATA-binding protein gene: a new polyglutamine disease? *Hum. Mol. Genet.*, **8**, 2047–2053.
27. Bois, P.R.J. (2003) Hypermutable minisatellites, a human affair? *Genomics*, **81**, 349–355.
28. Mangiarini, L., Sathasivam, K., Seller, M., Cozens, B., Harper, A., Hetherington, C., Lawton, M., Trottier, Y., Lehrach, H., Davies, S.W. and Bates, G.P. (1996) Exon 1 of the *HD* gene with an expanded CAG repeat is sufficient to cause a progressive neurological phenotype in transgenic mice. *Cell*, **87**, 493–506.
29. Hodgson, J.G., Agopyan, N., Gutekunst, C.A., Leavitt, B.R., LePiane, F., Singaraja, R., Smith, D.J., Bissada, N., McCutcheon, K., Nasir, J. *et al.* (1999) A YAC mouse model for Huntington's disease with full-length mutant huntingtin, cytoplasmic toxicity, and selective striatal neurodegeneration. *Neuron*, **23**, 181–192.
30. Usdin, M.T., Shelbourne, P.F., Myers, R.M. and Madison, D.V. (1999) Impaired synaptic plasticity in mice carrying the Huntington's disease mutation. *Hum. Mol. Genet.*, **8**, 839–846.
31. Murphy, K.P.S.J., Carter, R.J., Lione, L.A., Mangiarini, L., Mahal, A., Bates, G.P., Dunnett, S.B. and Morton, A.J. (2000) Abnormal synaptic plasticity and impaired spatial cognition in mice transgenic for exon 1 of the human Huntington's disease mutation. *J. Neurosci.*, **20**, 5115–5123.
32. Oyake, M., Onodera, O., Shiroishi, T., Takano, H., Takahashi, Y., Kominami, R., Moriwaki, K., Ikeuchi, T., Igarashi, S., Tanaka, H. and Tsuji, S. (1997) Molecular cloning of murine homologue dentatorubral–pallidoluysian atrophy (DRPLA) cDNA: strong conservation of a polymorphic CAG repeat in the murine gene. *Genomics*, **40**, 205–207.
33. Zhang, S., Xu, L., Lee, J. and Xu, T. (2002) *Drosophila* atrophin homolog functions as a transcriptional corepressor in multiple developmental processes. *Cell*, **108**, 45–56.
34. Sato, A., Shimohata, T., Koide, R., Takano, H., Sato, T., Oyake, M., Igarashi, S., Tanaka, K., Inuzuka, T., Nawa, H. and Tsuji, S. (1999) Adenovirus-mediated expression of mutant DRPLA proteins with expanded polyglutamine stretches in neuronally differentiated PC12 cells: preferential intranuclear aggregate formation and apoptosis. *Hum. Mol. Genet.*, **8**, 997–1006.
35. Nucifora, F.C. Jr., Ellerby, L.M., Wellington, C.L., Wood, J.D., Herring, W.J., Sawa, A., Hayden, M.R., Dawson, V.L., Dawson, T.M. and Ross, C.A. (2003) Nuclear localization of a non-caspase truncation product of atrophin-1, with an expanded polyglutamine repeat, increases cellular toxicity. *J. Biol. Chem.*, **278**, 13047–13055.
36. Koide, R., Onodera, O., Ikeuchi, T., Kondo, R., Tanaka, H., Tokiguchi, S., Tomoda, A., Miike, T., Isa, F., Beppu, H. *et al.* (1997) Atrophy of the cerebellum and brainstem in dentatorubral pallidoluysian atrophy: influence of CAG repeat size on MRI findings. *Neurology*, **49**, 1605–1612.
37. Colomer, V., Engelender, S., Sharp, A.H., Duan, K., Cooper, J.K., Lanahan, A., Lyford, G., Worley, P. and Ross, C.A. (1997) Huntingtin-associated protein 1 (HAP1) binds to a Trio-like polypeptide, with a rac1 guanine nucleotide exchange factor domain. *Hum. Mol. Genet.*, **6**, 1519–1525.
38. Ma, X.M., Huang, J., Wang, Y., Eipper, B.A. and Mains, R.E. (2003) Kalirin, a multifunctional Rho guanine nucleotide exchange factor, is necessary for maintenance of hippocampal pyramidal neuron dendrites and dendritic spines. *J. Neurosci.*, **23**, 10593–10603.
39. Luthi-Carter, R., Hanson, S.A., Strand, A.D., Bergstrom, D.A., Chun, W., Peters, N.L., Woods, A.M., Chan, E.Y., Kooperberg, C., Krainc, D. *et al.* (2002) Dysregulation of gene expression in the R6/2 model of polyglutamine disease: parallel changes in muscle and brain. *Hum. Mol. Genet.*, **11**, 1911–1926.
40. Shimohata, M., Shimohata, T., Igarashi, S., Naruse, S. and Tsuji, S. (2005) Interference of CREB-dependent transcriptional activation by expanded polyglutamine stretches—augmentation of transcriptional activation as a potential therapeutic strategy for polyglutamine diseases. *J. Neurochem.*, **93**, 654–663.
41. Mantamadiotis, T., Lemberger, T., Bleckmann, S.C., Kern, H., Kretz, O., Martin Villalba, A., Tronche, F., Kellendonk, C., Gau, D., Kapfhammer, J. *et al.* (2002) Disruption of CREB function in brain leads to neurodegeneration. *Nat. Genet.*, **31**, 47–54.
42. Zhai, W., Jeong, H., Cui, L., Krainc, D. and Tjian, R. (2005) *In vitro* analysis of huntingtin-mediated transcriptional repression reveals multiple transcription factor targets. *Cell*, **123**, 1241–1253.
43. Yamamoto, A., Lucas, J.J. and Hen, R. (2000) Reversal of neuropathology and motor dysfunction in a conditional model of Huntington's disease. *Cell*, **101**, 57–66.
44. Mazarakis, N.K., Cybulska-Klosowicz, A., Grote, H., Pang, T., Van Dellen, A., Kossut, M., Blakemore, C. and Hannan, A.J. (2005) Deficits in experience-dependent cortical plasticity and sensory-discrimination learning in presymptomatic Huntington's disease mice. *J. Neurosci.*, **25**, 3059–3066.
45. Kano, M., Hashimoto, K., Kurihara, H., Watanabe, M., Inoue, Y., Aiba, A. and Tonegawa, S. (1997) Persistent multiple climbing fiber innervation of cerebellar Purkinje cells in mice lacking mGluR1. *Neuron*, **18**, 71–79.
46. Shin, R.M., Masuda, M., Miura, M., Sano, H., Shirasawa, T., Song, W.J., Kobayashi, K. and Aosaki, T. (2003) Dopamine D4 receptor-induced postsynaptic inhibition of GABAergic currents in mouse globus pallidus neurons. *J. Neurosci.*, **23**, 11662–11672.

J Cutan Pathol 2009: 36: 517–521
doi: 10.1111/j.1600-0560.2008.01086.x
John Wiley & Sons. Printed in Singapore

Journal of
Cutaneous Pathology

Reduction in QSART and vasoactive intestinal polypeptide expression in the skin of Parkinson's disease patients and its relation to dyshidrosis

Background: With regards to dyshidrosis in Parkinson's disease (PD), there is no established and consistent view on the occurrence sites, frequency and etiology, although there have been several reports on hypohidrosis of the limbs and sudoresis on the face/cervical region.
Methods: Hydrosis in the forearms of PD patients and healthy individuals were compared by quantitative sudomotor axon reflex test (QSART). The expression of various neuropeptides and α-synuclein was examined with immunohistochemical staining.
Results: There was a significant reduction in QSART of PD patients but not of healthy controls. Reduced expression of vasoactive intestinal polypeptide (VIP) was also detected in the sweat glands of PD patients.
Conclusion: Reduction in QSART and VIP expression in the sweat glands might be involved in the dyshidrosis of PD patients.

Kawada M, Tamada Y, Simizu H, Yanagishita T, Yamashita N, Ishida N, Watanabe D, Yoshida M, Ibi T, Sahashi K, Hashizume Y, Matsumoto Y. Reduction in quantitative sudomotor axon reflex test and vasoactive intestinal polypeptide expression in the skin of Parkinson's disease patients and its relation to dyshidrosis.
J Cutan Pathol 2009; 36: 517–521. © 2009 John Wiley & Sons A/S.

Morihiro Kawada[1], Yasuhiko Tamada[1], Hirokazu Simizu[1], Takeshi Yanagishita[1], Noriko Yamashita[1], Natsuko Ishida[1], Daisuke Watanabe[1], Mari Yoshida[3], Tatsu Ibi[2], Kou Sahashi[2], Yoshio Hashizume[3] and Yoshinari Matsumoto[1]

[1]Department of Dermatology,
[2]Department of Neurology, Aichi Medical University School of Medicine, Nagakute, Aichi, Japan
[3]Department of Neurology, Institute for Medical Science of Aging, Aichi Medical University School of Medicine, Nagakute, Aichi, Japan

Daisuke Watanabe, Department of Dermatology, Aichi Medical University School of Medicine, Nagakute, Aichi 480-1195, Japan
Tel: +81 (52) 264-4811
Fax: +81 (561) 63-9914
e-mail: dwatanab@aichi-med-u.ac.jp

Accepted for publication May 18, 2008

Although dyshidrosis is widely known as one of the autonomic disorders in Parkinson's disease (PD), the frequency of the disorder varies among investigators' reports. Appenzeller et al.[1] and Aminoff et al.[2] found 10 disorders (53%) of 19 patients and 6 (54%) of 11 patients, respectively. Sandroni et al.[3] reported dyshidrosis in less than 40% of 35 PD patients. Thaisetthawatkul et al.[4] reported that PD patients had the mildest degree of the disorder. However, Kihara et al.[5] failed to show significant changes in hydrosis of PD patients. The varied frequency of incidence and intensity of dyshidrosis might be because of difference in techniques used or in disease stages of PD patients.

Sweat production is regulated by autonomic neural system, and the dyshidrosis in PD is suggested to be caused by autonomic neural disturbance, especially sympathetic nervous system.[6] Sweat gland is innervated by cholinergic sympathetic neurons.[7] The sympathetic nerve-dependent sweat production can be analyzed by a quantitative sudomotor axon reflex tests (QSART).[8] Immunohistochemical studies have identified a number of possible peptide neuromodulators (e.g. vasoactive intestinal polypeptide, VIP) in and around cholinergic sudomotor nerve terminals and eccrine sweat glands.[9,10] In this study, we examined dyshidrosis of PD patients with QSART on sympathetic nerve functions. We also examined the

expression of neuropeptides and α-synuclein, which affect sympathetic nerve functions, in the sweat glands of the patients with immunohistochemical staining.

Materials and methods

Subjects

Twelve PD patients who were under the care of the Department of Neurological Medicine in Aichi Medical University Hospital were the subjects. Of these, six patients were males (mean age 69.8 years) and six were females (mean age 69.7 years). The mean disease duration was 103.3 months. The control group consisted of six patients without a skin rash on the forearm, three males (mean age 66 years) and three females (mean age 67 years), who are under the care of the Department of Dermatology in the hospital. In addition, autopsy samples from three patients (two males and one female with a mean age of 72.8 years), who were pathologically diagnosed for having PD or diffuse Lewy body disease from 1995 to 2003 in the Institute for Aging, were utilized for staining of the sympathetic ganglia. All experiments were carried out under the consent of the patients and healthy controls.

Quantitative sudomotor axon reflex test

QSART was used to examine the integrity of post-ganglionic sympathetic cholinergic innervation of sweat glands.[7] Sweat production is measured in an adjacent area by the increase in relative humidity in an airtight chamber. Briefly, 10% acetylcholine was made to infiltrate the measurement site on the right forearm by iontophoresis for 5 min at 1 mA electric current, and the amount for the axon reflex sweating was quantified by using the capsule ventilation technique. This was recorded for 10 min as the axon reflex-mediated sweat response. Amount of perspiration (mg/10 min) is expressed as the mean ± SD. The statistical significance of differences was determined by unpaired Student's *t*-test. A $p < 0.05$ vs. control subjects was considered statistically significant.

Immunohistochemistry

Among 12 patients who were subjected to QSART, 3-mm punch biopsy specimens were obtained from the forearm flexor surface of 11 patients consented to this procedure. The specimens were fixed with formalin and stained with hematoxylin and eosin. They were also stained immunohistochemically with antibodies against the following antigens: neuron-specific enolase (NSE), protein gene product 9.5 (PGP9.5), choline acetyltransferase (ChAT), calcitonine gene-related peptide (CGRP) and VIP. After deparaffinization, the specimens were treated with 30% hydrogen peroxide, reacted with each primary antibody (Table 1) at 4°C for 24 h and stained using the labeled streptavidin-biotin method (DAKO, Glostrup, Denmark) according to manufacturer's protocol. Nuclei were stained with Mayer's hematoxylin. Three to five sweat gland secretory portions per specimen were observed under a microscope and the

Table 1. The list of antibodies used for immunohistochemical studies

Antibody	Source	Dilution used
NSE	Dako	1 : 200
PGP9.5	Dako	1 : 100
ChAT	Chemicon (CA, USA)	1 : 100
CGRP	Sigma (Mi, USA)	1 : 100
VIP	Sigma (Mi, USA)	1 : 100
α-Syn	Santa Cruz (CA, USA)	1 : 200
p-α-Syn	Wako (Osaka, Japan)	1 : 2000

α-Syn, α-synuclein; CGRP, P-α-Syn, phosphorylated α-synuclein; calcitonine gene-related peptide; ChAT, choline acetyltransferase; NSE, neuron-specific enolase; PGP, protein gene product; VIP, vasoactive intestinal polypeptide.

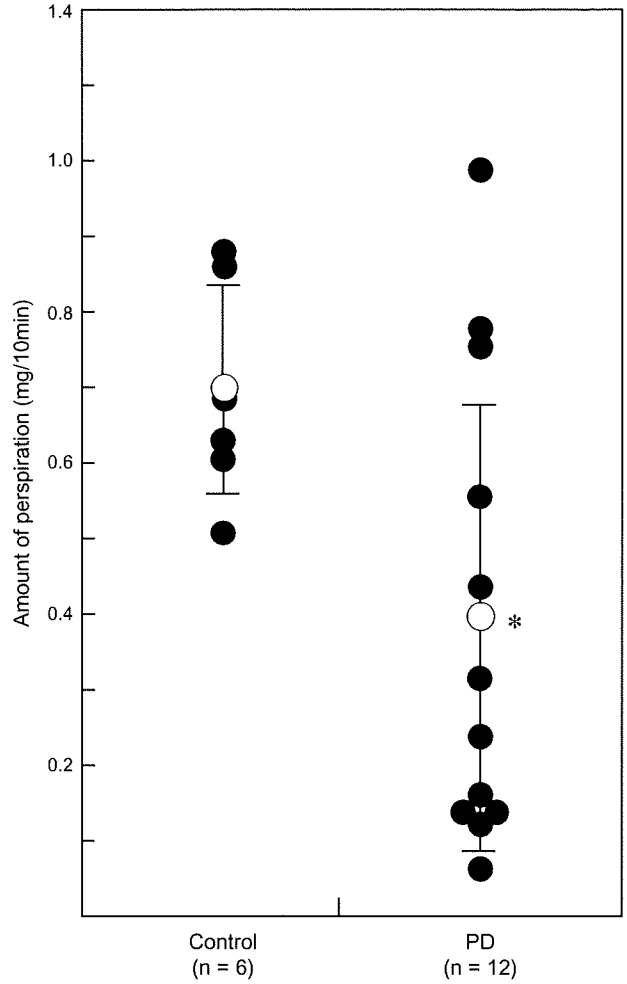

Fig. 1. Quantitative sudomotor axon reflex test. Axon reflex sweating of the upper limbs in Parkinson's disease patients and controls were examined ●. Amount of perspiration is expressed as the mean (white circle) ± SD. *$p < 0.05$ vs. control subjects.

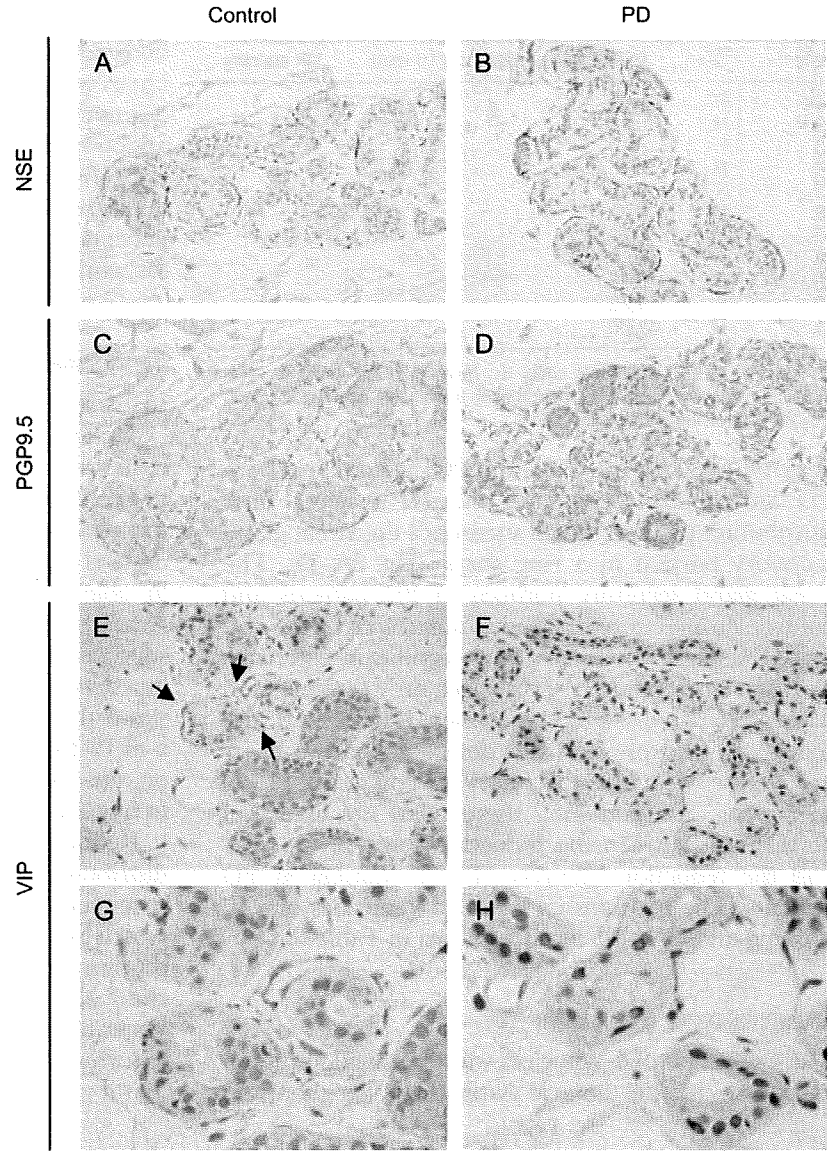

Fig. 2. Expression of neuropeptides in the sweat glands was examined with immunohistochemical staining. Original magnification: (A–F) ×400; (G and H) ×1000. NSE, neuron-specific enolase; PD, Parkinson's disease; PGP, protein gene product; VIP, vasoactive intestinal polypeptide.

staining was scored as negative (−), weak positive (±) or positive (+) based on the number of positive cells.[8] Formalin-fixed and paraffin-embedded sections (9 μm) of the autopsied sympathetic ganglia of the three PD patients and three control patients were immunohistochemically stained with anti-α-synuclein antibody and anti-phosphorylated α-synuclein antibody. Similar staining was also performed with the 4-μm skin sections.

Results

Quantitative sudomotor axon reflex test

QSART was carried out in 12 PD patients and six healthy controls (Fig. 1). Reduction in QSART was observed in 7 of 12 PD patients. The axon reflex sweating on the upper limbs of PD patients was significantly low compared with the case of the control subjects ($p < 0.05$).

Histology of the sweat glands

The histology of the sweat glands of PD patients and healthy controls was observed under a microscope. Neither the atrophy of the sweat gland secretory portions nor the constriction of the ducts was observed in PD patients (data not shown). There was no histological difference in the sweat glands between PD patients and the healthy controls.

Expression of neuropeptides in the sweat glands

The expression of various neuropeptides was examined immunohistochemically in the sweat glands of PD

Table 2. Comparison of the reduction in QSQRT and VIP expression

Patient	Sex	QSART perspiration (mg/10 min)	VIP staining
1	F	0.06	−
2	M	0.13	±
3	F	0.15	−
4	M	0.15	−
5	F	0.25	±
6	M	0.32	−
7	M	0.43	−
8	F	0.54	±
9	F	0.76	−
10	F	0.78	−
11	M	1.00	−

−, negative; ±, 1–4 positive cells; +, more than five positive cells; F, female; M, male; QSART, quantitative sudomotor axon reflex test; VIP, vasoactive intestinal polypeptide.

patients (Fig. 2). In the NSE and PGP9.5 staining, both PD and control specimens showed a nerve fiber distribution pattern, which surrounds the sweat gland secretory portion in a ring shape (Fig. 2A–D). The sweat gland secretory portions in PD patients and control samples were positively stained with ChAT and CGRP staining and there was no significant difference in those staining patterns. However, no VIP expression was detected in 8 of 11 PD specimens (Fig. 2E–H), and reduced VIP expression was detected at nerve fibers around the sweat gland secretory portion in 3 of 11 PD specimens. In addition, there was no statistical correlation between the reduction score of QSART and the reduction intensity of VIP staining in PD patients. The relationship between intensities of VIP staining and QSART levels is shown in Table 2.

Accumulation of α-synuclein

The expression of α-synuclein was examined immunohistochemically in thoracic sympathetic ganglion and sweat glands of PD patients. Nerve cells and nerve cell bodies of the sympathetic ganglia in the PD autopsy specimens were positively stained with anti-phosphorylated α-synuclein antibody (Fig. 3A) and anti-α-synuclein antibody (data not shown). However, no positive staining was observed in skin specimens collected from the forearms of the 11 PD patients and autopsied control patients (Fig. 3B–D). The summary of the immunohistochemical stainings is shown in Table 3.

Discussion

In this study, we show the reduction in QSART and VIP expression in the sweat glands of PD patients. The reduction in QSART and VIP expression might be involved in the dyshidrosis of PD patients. QSART is a sympathetic nerve-dependent hidrosis testing method devised by Low et al., which was judged to be excellent in objectivity and reproducibility by the American Academy of Neurology.[11] The reduction in QSART suggests the involvement of altered sympathetic nerve function in the dyshidrosis of PD patients. This study shows the reduced sweating function on the forearm in 6 of 12 PD patients. There are already several reports on the dyshidrosis of PD patients,[1–5] although the frequency and intensity varied in those reports.

Reduced VIP expression is seen in the nerves distributed around the secretory portion of the PD specimens. VIP is normally expressed in the dermal vessels and the nerves around the sweat gland secretory portion and plays an important role in hidrosis along with acetylcholine.[12] Using eccrine sweat glands separated from a Rhesus monkey's palm, Sato et al.[13] reported that VIP induces eccrine perspiration and that it accumulates cyclic adenosine mono-phosphate

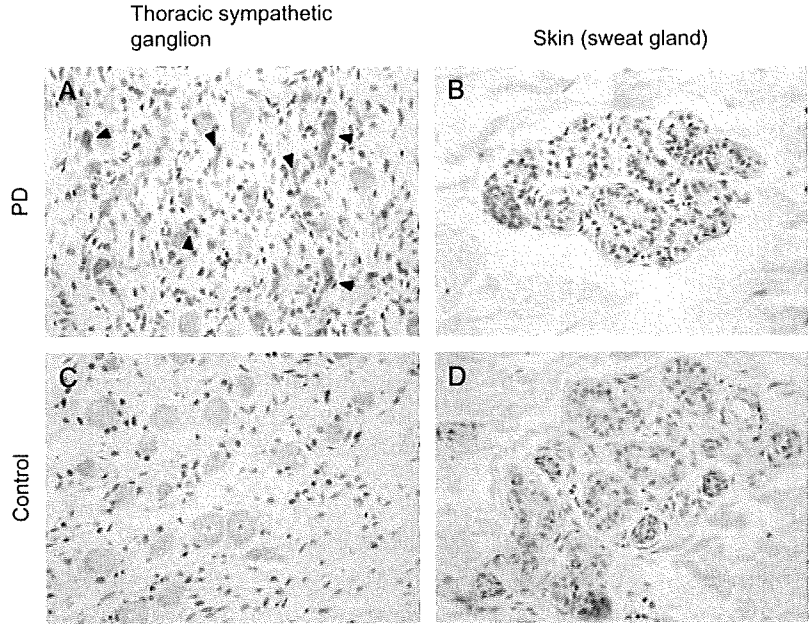

Fig. 3. A–D) Expression of α-synuclein in the sweat glands was examined with immunohistochemical staining. Original magnification ×400. PD, Parkinson's disease.

Table 3. The summary of immunohistochemical staining

		Neuropeptide						
	Tissue	NSE	PGP	ChAT	CGRP	VIP	α-Syn	p-α-Syn
Control	Skin	+	+	+	±	+	−	−
	Thoracic sympathetic ganglion						−	−
Parkinson's disease	Skin	+	+	+	±	−∼± (3/11: ±) (8/11: −)	−	−
	Thoracic sympathetic ganglion						+	+

α-Syn, α-synuclein; P-α-Syn, phosphorylated α-synuclein; CGRP, calcitonine gene-related peptide; ChAT, choline acetyltransferase; PGP, protein gene product; NSE, neuron-specific enolase; VIP, vasoactive intestinal polypeptide.

(AMP) in the secretory cells and increases the secretion of sweat. Moreover, Tainio[14] confirmed that VIP activates adenylate cyclase even without synergy from acetylcholine in the human sweat glands and promotes cyclic adenosine mono-phosphate (cAMP) production from adenosine tri-phosphate (ATP). Further, the relationship between dyshidrosis and reduced VIP expression is known in several diseases.[15,16] Based on those findings, the reduced VIP expression in the sweat glands of PD patients might be related to the altered sympathetic nerve function, assessed by QSART.

The appearance of Lewy bodies in the sympathetic nervous system leads to autonomic nervous system dysfunction.[17-19] No deposit of α-synuclein was observed in the sweat glands of PD patients, although it was observed in the nerve cells and neurites of the thoracic sympathetic ganglia. In this study, we could not obtain the evidence on the dysfunction of sympathetic nerves in the sweat glands by α-synuclein. However, a possibility is not excluded that the accumulation of α-synuclein in the thoracic sympathetic ganglia might play a role on the dyshidrosis in PD.

Neither the atrophy of the sweat gland secretory portions nor the constriction of the ducts was seen in the sweat glands of PD patients. There was no significant difference in the histology of the sweat glands between PD patients and healthy controls. Therefore, the dyshidrosis of PD might be responsible for functional disorder of the perspiration nerve. It is also supported by the reduction in QSART and VIP expression.

Acknowledgements

We thank A. Morikawa, K. Kohtani and T. Mizuno for excellent technical assistance during the course of this study.

References

1. Appenzeller O, Gross JE. Autonomic deficits in Parkinson's syndrome. Arch Neurol 1971; 24: 50.
2. Aminoff MJ, Willcox CS. Assessment of autonomic function in patients with a Parkinsonian syndrome. Br Med J 1971; 4: 80.
3. Sandroni P, Ahlskog JE, Fealey RD, Low PA. Autonomic involvement in extrapyramidal and cerebellar disorders. Clin Auton Res 1991; 1: 147.
4. Thaisetthawatkul P, Boeve BF, Benarroch EE, et al. Autonomic dysfunction in dementia with Lewy bodies. Neurology 2004; 62: 1804.
5. Kihara M, Kihara Y, Tukamoto T, et al. Assessment of sudomotor dysfunction in early Parkinson's disease. Eur Neurol 1993; 33: 363.
6. Hirayama M. Sweating dysfunctions in Parkinson's disease. J Neurol 2006; 253: 42.
7. Ernsberger U, Rohrer H. Development of the cholinergic neurotransmitter phenotype in postganglionic sympathetic neurons. Cell Tissue Res 1999; 297: 339.
8. Braune C, Erbguth F, Birklein F. Dose thresholds and duration of the local anhidrotic effect of botulinum toxin injections: measured by sudometry. Br J Dermatol 2001; 144: 111.
9. Tainio H, Vaalasti A, Rechadt L. The distribution of substance P-, CGRP-, galanin- and ANP-like immunoreactive nerves in human sweat glands. Histochem J 1987; 19: 375.
10. Shibasaki M, Wilson TE, Crandall CG. Neural control and mechanisms of eccrine sweating during heat stress and exercise. J Appl Physiol 2006; 100: 1692.
11. Low PA, Caskey PE, Tuck RR, Fealey RD, Dyck PJ. Quantitative sudomotor axon reflex test in normal and neuropathic subjects. Ann Neurol 1983; 14: 573.
12. Lotti T, Hautmann G, Panconesi E. Neuropeptides in skin. J Am Acad Dermatol 1995; 33: 482.
13. Sato K, Sato F. Effect of VIP on sweat secretion and cAMP accumulation in isolated simian eccrine glands. Am J Physiol 1987; 253: R935.
14. Tainio H. Cytochemical localization of VIP-stimulated adenylate cyclase activity in human sweat glands. Br J Dermatol 1987; 116: 323.
15. Properzi G, Francavilla S, Poccia G, et al. Early increase precedes a depletion of VIP and PGP-9.5 in the skin of insulin-dependent diabetics – correlation between quantitative immunohistochemistry and clinical assessment of peripheral neuropathy. J Pathol 1993; 169: 269.
16. Nolano M, Provitera V, Perretti A, et al. Ross syndrome: a rare or a misknown disorder of thermoregulation? A skin innervation study on 12 subjects. Brain 2006; 129: 2119.
17. Den Hartog Jager WA, Bethlem J. The distribution of Lewy bodies in the central and peripheral autonomic nervous systems in idiopathic paralysis agitans. J Neurol Neurosurg Psychiatry 1960; 23: 283.
18. Rajput AH, Rozdilsky B. Dysautonomia in Parkinsonism: a clinicopathological study. J Neurol Neurosurg Psychiatry 1976; 39: 1092.
19. Hague K, Lento P, Morgello S, Caro S, Kaufmann H. The distribution of Lewy bodies in pure autonomic failure: autopsy findings and review of the literature. Acta Neuropathol 1997; 94: 192.

NEUROPATHOLOGY

Neuropathology 2009; **29**, 697–703 doi:10.1111/j.1440-1789.2009.01003.x

Case Report

An autopsy case of diffuse neurofibrillary tangles with calcification: Early stage pathologic findings

Yasushi Iwasaki,[1] Masumi Ito,[1] Keiko Mori,[1] Akira Deguchi,[2] Masamitsu Nagaoka,[3] Mari Yoshida[4] and Yoshio Hashizume[4]

Departments of [1]Neurology, [2]Internal Medicine and [3]Pathology, Oyamada Memorial Spa Hospital, Yokkaichi, and [4]Department of Neuropathology, Institute for Medical Science of Aging, Aichi Medical University, Aichi, Japan

A 66-year-old man with no medically remarkable past or family history gradually showed personality changes, memory disturbance, sleeplessness and abnormal behavior. Neurologic examination showed no focal signs and neither parkinsonism nor cerebellar ataxia was recognized. He died 4 years after the onset of dementia due to chronic renal failure. Neuropathologic examination revealed neuronal loss and gliosis in the temporal cortex, particularly in the subiculum, parahippocampal gyrus and entorhinal cortex, and insular cortex. NFTs were observed to be widespread in the cerebral cortex, especially the temporal cortex and brainstem, while senile plaques were not observed. Gallyas-Braak silver staining revealed the presence of numerous NFTs, glial inclusions and neuropil threads throughout the cerebral neocortex, limbic system, hippocampus and brainstem. The subiculum showed the most severe involvement; severe atrophy, severe neuron loss, and numerous ghost tangles (extracellular NFTs) were apparent. Although NFTs contained both monoclonal anti-3repeat-tau antibody (RD3) and RD4 immunoreactivity, this differed between the intracellular NFTs and ghost tangles. RD3 immunoreactivity was mainly observed in ghost tangles and neuropil threads, whereas RD4 immunoreactivity was mainly observed in intracellular NFTs and glial inclusions. Calcification was also found to be widespread in the cerebral cortex and white matter, basal ganglia, thalamus, cerebellar cortex, white matter and dentate nucleus. These characteristic neuropathologic findings lead to the pathologic diagnosis of diffuse neurofibrillary tangles with calcification (DNTC). It is argued that this patient showed early stage pathologic signs of DNTC due to a short disease duration, which may provide clues regarding the progression of this rare disease.

Key words: calcification, diffuse neurofibrillary tangles with calcification, glial inclusion, neurofibrillary tangle, neuropil thread.

INTRODUCTION

Diffuse neurofibrillary tangles with calcification (DNTC) represents a primary sporadic dementia that is characterized by temporal-dominant cerebral atrophy with numerous NFTs, glial inclusions, neuropil threads and widespread calcification without senile plaques.[1–4] DNTC was first described as a rare tangle-predominant presenile dementia by Kosaka[1] and Shibayama.[2] A majority of reported cases are in Japanese individuals with no apparent family history of the disease.[1–3] In general, DNTC shows a slow progression and is associated with behavioral change, memory disturbance, hallucination and sometimes parkinsonism.[1–3] DNTC patients are understood to become bedridden and subsequently die after a median period of approximately 10 years.[1–3]

Diffuse neurofibrillary tangles with calcification is largely understood to affect people of Japanese descent and only about 20 autopsied cases have been recorded. Furthermore, there is no detailed case report regarding the clinicopathologic findings of DNTC. This research outlines an autopsy performed on a DNTC case which has not been previously reported. It is believed that this patient represents an individual affected at the onset or early stage of DNTC due to a relatively short disease duration of 4 years, and therefore the individual may provide clues regarding the pathologic progression of this rare disease. A discussion of the clinicopathologic aspects of the case with respect to DNTC phenotypic variability includes clinical findings, tau pathology and ultrastructural examination.

Correspondence: Yasushi Iwasaki, MD, Department of Neurology, Oyamada Memorial Spa Hospital, 5538-1 Yamada-cho, Yokkaichi 512-1111, Japan. Email: iwasaki@sc4.so-net.ne.jp

Received 23 August 2008; revised 20 December 2008 and accepted 21 December 2008; published online 5 March 2009.

CLINICAL SUMMARY

A 66-year-old Japanese man with no medically remarkable past or family history was transferred to the Department of Internal Medicine at the Oyamada Memorial Spa Hospital, Japan, due to the onset of dementia with chronic renal failure. The patient had graduated from a senior high school and is understood to have been socially active, but in the few months prior to being transferred, he showed personality changes in the form of aggression, irritability and being more easily agitated. The patient was also afflicted with memory disturbance, sleeplessness and abnormal behavior including wandering, restlessness and confusion. His speech was fluent and his ability to hold a conversation was maintained. Although his co-operation with medical examinations was relatively good, disorientation was apparent, and there was no recognition of the illness from the patient. Urinary incontinence was also observed. Focal signs including aphasia and hemiparesis, oral tendency, parkinsonism and cerebellar dysfunction were not observed. There were no apparent motor or sensory abnormalities of the extremities. Tendon reflexes were normal and Babinski signs were not present. Blood biochemistry observations including calcium and phosphorus values were free from abnormalities with the exception of blood urea nitrogen and creatinine, which were increased. Lues reaction was negative. The clinical diagnosis was senile psychosis.

In a gradual progression of the changes noted in the patient's behavior, he eventually started to commit acts of intense domestic violence against his wife. Sleeplessness became severe, and wandering also worsened. Antidepressant and antipsychotic drugs were administered at this stage, but neuropsychologic symptoms and signs had not improved. Although psychological and neurological symptoms gradually progressed, normal activities of daily living were maintained until shortly before death. The antipsychotic drug was discontinued because of renal dysfunction. He died at the age of 70, 4 years after the onset of dementia, due to chronic renal failure. Pyramidal signs and extrapyramidal signs were not observed throughout the clinical course. Head CT scan and MRI were not performed.

METHODS

Neuropathologic examination

The brain was removed 12 h after death and immersed in 20% neutral buffered formalin. Spinal cord samples were not available. The tissues were embedded in paraffin and cut into 8-μm thick sections. For routine histological examination, each section was stained with HE, KB, methenamine silver and, after pretreatment with 0.3% KMnO4, Gallyas-Braak (G-B) silver staining. The Berlin-blue staining for iron, Dahl's staining and von Kossa's staining for calcium were also performed. The distribution of neurofibrillary pathology was determined according to Braak *et al.*[5]

Immunohistochemical staining of tau isoforms was performed with RD3 (monoclonal anti-3repeat-tau antibody, 1:500, clone 8E6/C11; Upstate Biotechnology, Lake Placid, NY, USA) and RD4 (monoclonal anti-4repeat-tau antibody, 1:200, clone 1E1/A6; Upstate Biotechnology), in addition to phosphorylation-dependent tau epitopes (AT-8, monoclonal, 1:1000; Innogenetics, Ghent, Belgium) antibodies by the avidin-biotin-peroxidase complex method with 3.3-diaminobenzidinetetrahydrochloride as chromogen. RD3 and RD4 immunoreactivity were applied after pretreatment of the sections in a microwave oven and formic acid for 10 min. α-synuclein (polyclonal, at 1:400; Santa Cruz Biotechnology, Santa Cruz, CA, USA) and β-amyloid (monoclonal, at 1:100; DAKO, Glostrup, Denmark) antibodies were also used where appropriate. The immunolabelled sections were counterstained lightly with hematoxylin.

The sections of subiculum were used for electron microscopy. The sections were washed in phosphate buffer, post-fixed with 1% osmium tetroxide, dehydrated in a graded series of ethanol and embedded in Epon. Ultrathin sections were stained with uranyl acetate and lead citrate. The sections were then cut into 70-nm slices, and examined with an electron microscope at 75 kV (Hitachi H-7000, Tokyo, Japan).

PATHOLOGIC FINDINGS

Macroscopic findings

The brain weight at autopsy was 1100 g. The cerebral coronally cut surfaces showed temporal lobe atrophy (Fig. 1), but no frontal, parietal, occipial lobe, cerebellar or brainstem atrophy. Temporal lobe atrophy was apparently dominant at the subiculum with the observation of a brownish discoloration and the mild atrophied area extended over the entire temporal lobe, including the superior, middle and inferior temporal gyrus, hippocampus and parahippocampal gyrus. The basal ganglia, thalamus and cerebral white matter showed no abnormality. Dilatation of the lateral ventricles, predominantly in the inferior horns, was also observed. The vessels of the brain showed no gross abnormalities.

Microscopic findings

Mild to severe neuron loss with gliosis was observed in the temporal cortex and insular cortex. Most severe neuron

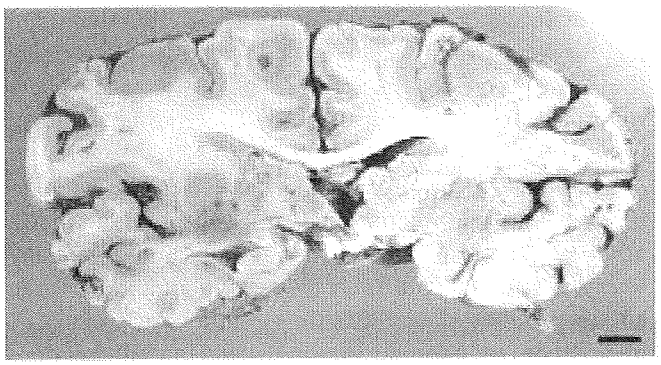

Fig. 1 Macroscopic findings of coronal section of the cerebral hemisphere. Subiculum is severely atrophic. Mild cortical atrophy is also observed in the temporal neocortex and the hippocampus. Inferior horns of the lateral ventricles are enlarged. The frontal lobe, striatum and thalamus are well preserved. Scale bar, 1 cm.

loss was observed in the subiculum to Cornu ammonis (CA)1 regions. In the subiculum, neuron loss was severe and numerous extracellular NFTs (ghost tangles) were observed (Fig. 2a). Mild loss of myelin and gliosis were present in the white matter of the temporal convolutions and insular gyrus. Spongiform change was observed in the II to III layers of the insular cortex. Hypertrophic astrocytosis was not so apparent in these affected regions. Some plaque-like structures[6] were found around small vessels in the temporal lobe, particularly in deep layers of the cortex and subcortical white matter, and a few were detected in the deep white matter. G-B silver staining revealed that the presence of numerous NFTs, glial inclusions and neuropil threads was widespread throughout the cerebral gray matter, particularly in the frontal (Fig. 3a) and temporal cortex, subiculum (Fig. 2b), hippocampus, amygdala, cingulate gyrus (Fig. 3b), claustrum, medial thalamus (Fig. 3c), mamillary body and insular cortex. In the caudate nucleus, putamen, globus pallidus, lateral thalamus and subthalamic nucleus, G-B-positive structures were relatively few in number. Glial inclusions showed coiled bodies while starlike-inclusions were thorn-shaped and tuft-shaped. Coiled bodies were suggested in oligodendrocytes and starlike-inclusions were in astrocytes, morphologically. Although the cerebellar cortex and white matter showed no apparent positivity with G-B silver staining, the dentate nucleus showed some NFTs, glial inclusions and neuropil threads. NFTs were also observed in the pontine nucleus, pontine tegmentum (Fig. 3d), locus ceruleus and substantia nigra, while no neuron loss was observed in the brainstem regions. The Braak's NFTs stage was V. In contrast with the widespread occurrence of NFTs, no senile plaques were detected by methenamine silver staining. Lewy bodies, neurites and Pick bodies were not observed.

Considerable precipitates of calcium-based substances were also observed to be widespread in the cerebral cortex and white matter, putamen, globus pallidus, thalamus and cerebellum (granule cell layer, white matter and dentate nuclei) (Figs 4,5a). These calcium depositions were observed in the parenchyma, and also in the walls of capillaries and arterioles. Although von Kossa's staining showed only a weak stain (Fig. 5b), Dahl's staining showed apparent positivity in these calcifications (Fig. 5c). Berlin-blue staining also showed apparent positivity which suggested the occurrence of iron accumulation in these calcifications (Fig. 5d). These calcium substances were not stained by G-B silver staining. Calcifications were not related with neuron loss, gliosis or presence of NFTs.

Immunohistochemical findings

AT-8 immunostaining also revealed diffuse and abundant NFTs, glial inclusions and neuropil threads in the cerebral cortex and brainstem. AT-8 gave the strongest staining, recognizing intracellular NFTs and neuropil threads. Ghost tangles were well identified by RD3 (Fig. 2c) and poorly stained by RD4 (Fig. 2d); they demonstrated decreased staining intensity for AT-8. Intracellular NFTs were positive for both RD3 and RD4; they were well-identified by RD4. RD3 immunoreactive intracellular NFTs were of dense oval or lump-shaped appearance, while RD4 immunoreactive intracellular NFTs demonstrated a fibrous flame-shaped appearance. Neuropil threads were predominantly stained for RD3 (Fig. 2c), and a small amount of neuropil threads were also positive for RD4 (Fig. 2d). Coiled bodies in oligodendroglias and astrocytic inclusions were also positive for RD4 immunostaining (Fig. 2d). No amyloid plaques were observed to react with the anti-β-amyloid antibodies, and α-synuclein positive structures were not found.

Calcium deposition was not stained by anti-tau (AT-8, RD3 and RD4), anti-α-synuclein or anti-β-protein immunostaining.

Electron microscopy

Straight fibrils were mainly observed in the NFTs located in the subiculum (Fig. 6a,b). Some paired helical filaments were also found (Fig. 6c).

DISCUSSION

We believe this case should be diagnosed as DNTC based on the following pathologic findings: temporal dominant lobar atrophy and lateral ventricular dilatation; presence of numerous NFTs throughout the cerebral gray matter and brainstem; widespread pathologic calcification in the cerebrum and cerebellum and the absence of senile plaques. No other neuropathologic features suggestive of complications arising from other neurological disorders, including

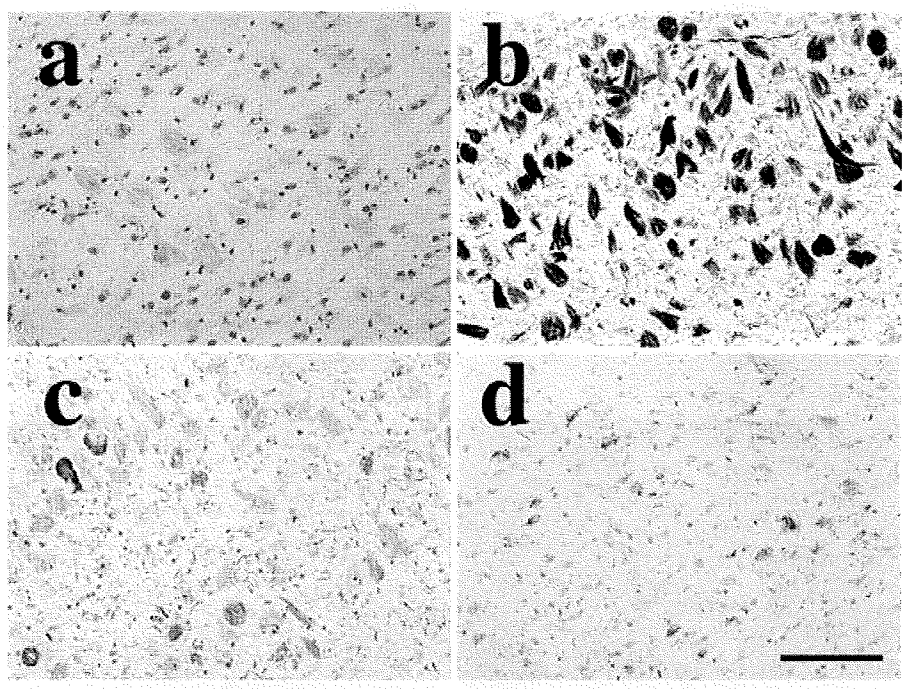

Fig. 2 Representative microscopic images of the subiculum. (a) Neurons are severely reduced in number. Numerous ghost tangles are recognized. (b) Numerous NFTs and neuropil threads are observed (c) Numerous RD3 (anti-3repeat-tau antibody)-positive structures are observed in the ghost tangles and neuropil threads. (d) Smaller numbers of RD4 (anti-4repeat-tau antibody)-positive flame-shaped NFTs are also recognized. Coiled bodies in oligodendroglias and astrocytic inclusions are also positive for RD4 immunostaining. Some RD4-positive neuropil threads are observed. Scale bar, 100 μm. a, KB staining; b, Gallyas-Braak silver staining; c, RD3 immunostaining; d, RD4 immunostaining.

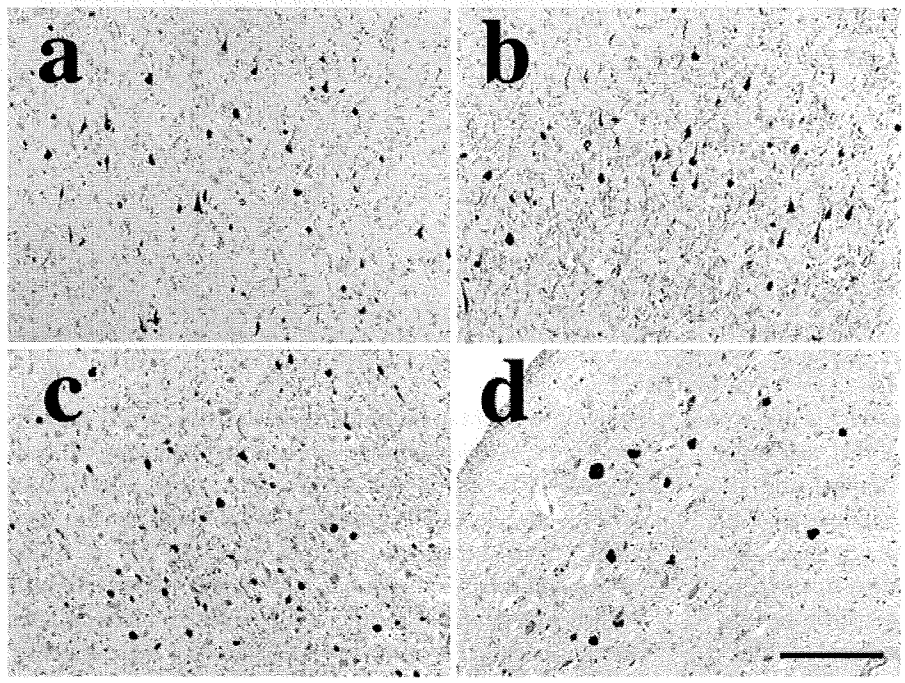

Fig. 3 NFTs in the representative regions. Many glial inclusions and neuropil threads are also observed. (a) Frontal neocortex; (b) cingulate gyrus; (c) medial thalamus; (d) pontine tegmentum (superior central nucleus). Gallyas-Braak silver staining. Scale bar, 200 μm.

Pick's disease and dementia with Lewy bodies, were evident. We also believe that this patient showed the early stages of DNTC pathologic findings due to a short disease duration of 4 years. The patient may therefore provide clues regarding the pathologic progression of this rare disease.

Diffuse neurofibrillary tangles with calcification has been considered an extremely rare entity of a slowly progressive presenile dementia involving memory disturbance and frontotemporal symptoms. However, it is asserted that DNTC may occur more frequently than generally reported because DNTC patients are often clinically misdiagnosed as suffering from Alzheimer's disease or Pick's disease.[2] Shibayama *et al.*[2] pointed out that the early stages of DNTC resemble Alzheimer's disease in that the patient's personality and mobility are maintained. However, the

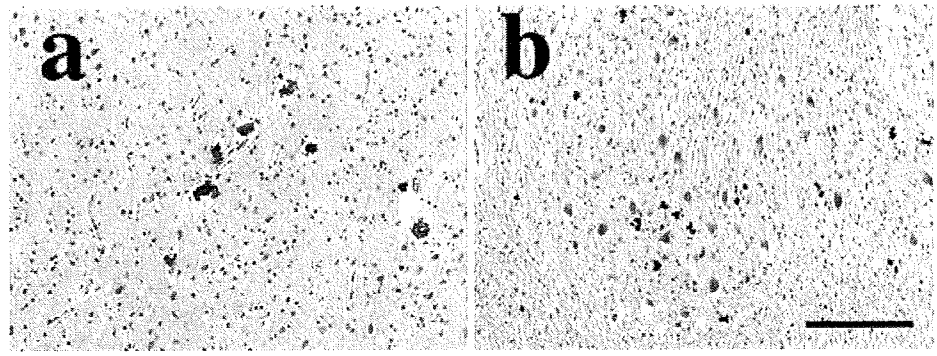

Fig. 4 Calcium deposition in the representative lesions. These cartifications are observed in the parenchyma, and also in the walls of capillaries and arterioles. (a) Frontal neocortex; (b) dentate nucleus of cerebellum. HE staining. Scale bar, 200 μm.

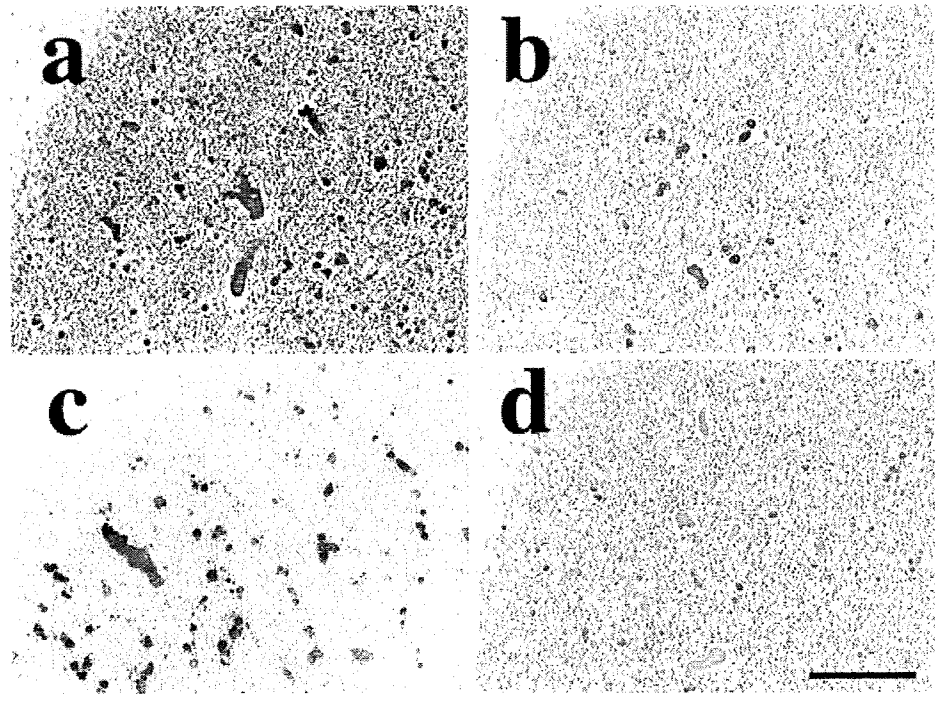

Fig. 5 Calcium deposition of the cerebellar cortex. HE staining, Dahl's staining and Berlin-blue staining show apparent positivity in the calcifications. Von Kossa's staining shows a particularly weak effect. (a) HE staining; (b) Von Kossa's staining; (c) Dahl's staining; (d) Berlin-blue staining. Scale bar, 200 μm.

course of the disease entails an accrual of Pick's disease-like symptoms of frontotemporal dementia such as apathy, disinhibited behavior, and personality change, and the disease is eventually characterized by a mixture of both sets of symptoms. Symptoms of the present case resembled Alzheimer's disease with the onset of memory disturbance and relatively normal mobility. At the same time, personality change and abnormal behavior resembled Pick's disease. Although, apraxia and agnosia were not recognized, these findings are compatible with other reports regarding DNTC.[2,3]

Neurodegenerative diseases with pathologic inclusions containing fibrillary aggregates of tau protein, collectively termed tauopathies, include both sporadic and familial disorders.[7] In sporadic tauopathies, including DNTC, the accumulation of abnormally phosphorylated tau in neurons and glias constitutes characteristic inclusions and regional distributions, respectively.[7] G-B silver staining and phosphorylated tau immunohistochemistry clearly demonstrate tau-positive inclusions in neurons and glias.[7] Flame-shaped NFTs in the cell bodies and apical dendrites of neurons and neuropil threads in distal dendrites are considered characteristic features of DNTC.[7] In DNTC, coiled bodies and starlike-inclusions both thorn-shaped and tuft-shaped are detected in the most severely affected sites (the temporal and limbic lobes) suggesting the possibility that glial inclusions are secondary formations by neuronal degeneration.[7,8]

Tau protein exists as six isoforms in the normal adult human brain.[9] A comparative biochemical study of tau aggregates has shown that these isoforms differ with regard to both the level of phosphorylation and content.[9] We used two characteristic monoclonal antibodies in the present study; RD3 (anti-3repeat-tau antibody) and RD4 (anti-4repeat-tau antibody). Although NFT contained both RD3 and RD4, immunoreactivity of these differed between

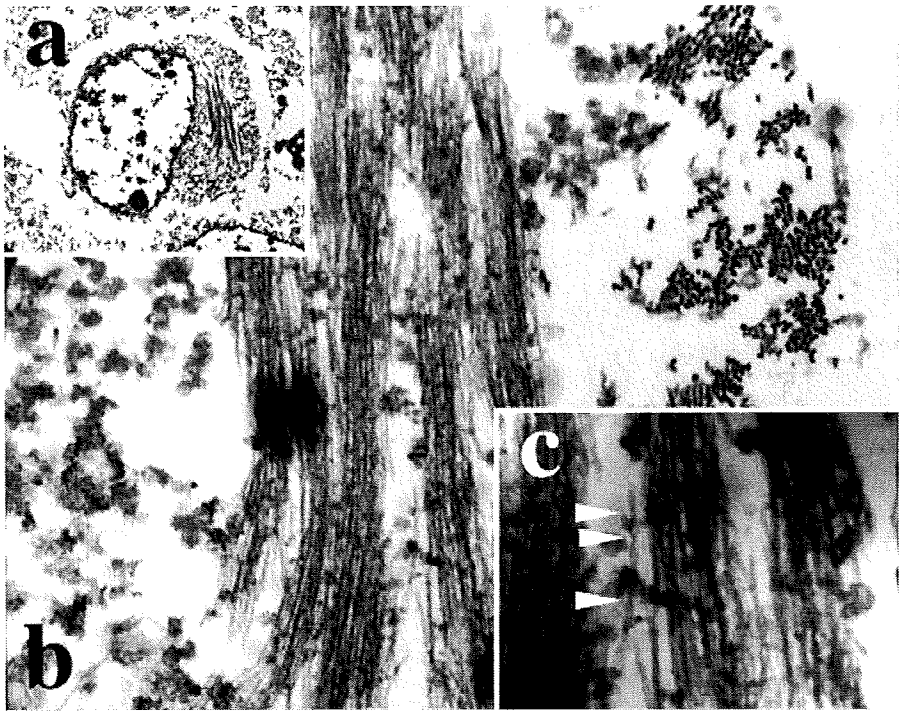

Fig. 6 Electromicrograph of NFTs in the subiculum. (a) Fibrils are recognized near the nucleus; (b) straight fibrils are mainly observed; (c) some paired helical filaments are also observed (indicated with arrowheads). (a) 3500×; (b) 30 000×; (c) 100 000×.

intracellular NFTs and ghost tangles. Intracellular NFTs were both positive in RD3 and RD4 but particularly well-identified by RD4. In the case of ghost tangles, RD3 immunoreactivity was more predominant. Furthermore, RD3 immunoreactivity was distinctive in neuropil threads, whereas RD4 immunoreactivity was distinctive in glial inclusions. Thus, tau-positive structures demonstrated heterogeneity and it is suggested that the isoform composition of DNTC may have a spectrum. In more advanced stages of DNTC cases, the immunoreactivity of tau isoforms may reflect proteolysis or modification of tau proteins in the disease process.[7] However, an immunohistochemical study of tau accumulation in early stages of Alzheimer-type neurofibrillary lesions revealed no specific tau isoform patterns.[10] Tanabe *et al.*[11] reported that ghost tangles were immunoreactive for the beta-amyloid 40 (Aβ40) in both DNTC and Alzheimer's disease, which could mean that Aβ40 deposition is a secondary phenomenon.

In DNTC, NFTs are widespread in the cerebral cortex, particularly in the temporal cortex and hippocampus, as well as the brainstem, while senile plaques are only present in small numbers.[1-3] Also, the strong correlation between regions of prolific NFTs and regions of intense neuron loss and atrophy in DNTC suggests that NFTs are the primary component of the pathology.[1-3] These findings also suggest that NFTs with neuron loss strongly contribute to clinical symptoms such as dementia. According to the distribution and degree of the degenerative lesions of the present case, we speculate that the pathologic progression of DNTC begins from the subiculum, before spreading to the limbic system, particularly in the insular cortex, hippocampus and entorhinal cortex.

Yokota *et al.*[12] investigated DNTC brains using immunohistochemistry and demonstrated remarkable α-synuclein deposition: Lewy bodies were in the neurons and astrocytes in many anatomical regions including the amygdala and hippocampus and, to a lesser degree, in the substantia nigra and dorsal vagal nucleus. The distribution pattern of α-synuclein-immunoreactive structures differed from that observed in Parkinson's disease and dementia with Lewy bodies.[12] It is likely that α-synuclein protein tends to accumulate in the regions where NFTs were most often observed.[12] Because no α-synuclein-positive structure was observed in the present case, we speculate that α-synuclein-positive structures are developed in progressive pathologic stages of DNTC.

Widespread calcification, particularly occurring in the basal ganglia and the dentate nucleus of the cerebellum, is one of the most characteristic features of DNTC.[1-3] Interestingly, this present case showed only a weakly positive result for Kossa's staining for calcium, but apparent positivities of Dahl's staining for calcium and Berlin-blue staining for iron. Ujihira *et al.*[3] used analytical electron microscopy to demonstrate accumulation of both iron and calcium in DNTC calcifications. In the present case, no apparent degeneration and neuron loss in the basal ganglia and cerebellum were observed, despite distinct calcification in these areas. Tsuchiya *et al.*[13] also suggested the same

findings. This finding shows that cellular function was maintained despite severe calcification, strongly indicating that calcification and neuronal degeneration occur independently in DNTC. Furthermore, the relationship between the distribution pattern of NFTs and calcification was not observed. It may be argued that clinical presentation is not influenced by calcification, because parkinsonism and cerebellar ataxia were not identified in the present case.

The filaments of NFTs from DNTC brains appeared structurally identical to the paired helical filaments observed in Alzheimer's disease that have been reported by ultrastructural examination.[3,11] In Alzheimer's disease, about 95% of tau filaments are in the form of paired helical filaments, and the remainder consists of straight fibrils. The present case showed that a majority of the filaments in NFTs showed straight fibrils. It is argued that DNTC may provide a unique opportunity to determine the role that tau-rich NFTs, glial inclusions and neuropil threads play in the dysfunction and degeneration of neurons in tauopathies.

We consider this patient to have shown the early-stage pathologic findings of DNTC due to a short disease duration. We speculate that the pathologic progression of DNTC begins from the subiculum before spreading to the limbic system, and that α-synuclein-positive structures are developed in progressive pathologic stages of DNTC. Furthermore, tau-positive structures demonstrated heterogeneity and it is suggested that the isoform composition of DNTC may have a spectrum.

REFERENCES

1. Kosaka K. Diffuse neurofibrillary tangles with calcification: a new presenile dementia. *J Neurol Neurosurg Psychiatry* 1994; **57**: 594–596.
2. Shibayama H, Kobayashi H, Nakagawa M *et al.* Non-Alzheimer non-Pick dementia with Fahr's syndrome. *Clin Neuropathol* 1992; **11**: 237–250.
3. Ujihira N, Hashizume Y, Takagi T, Ito M. An autopsied case of atypical presenile dementia which shows lobar atrophy, severe neurofibrillary tangles and calcification. *Rinsho shinkeigaku* 1997; **37**: 292–299. (In Japanese with English abstract).
4. Jellinger KA, Bancher C. Senile dementia with tangles (tangle predominant form of senile dementia). *Brain Pathol* 1998; **8**: 367–376.
5. Braak H, Braak E. Neuropathological stageing of Alzheimer-related changes. *Acta Neuropathol (Berl)* 1991; **82**: 239–259.
6. Terada S, Ishizu H, Tanabe Y *et al.* Plaque-like structures and arteriosclerotic changes in "diffuse neurofibrillary tangles with calcification" (DNTC). *Acta Neuropathol (Berl)* 2001; **102**: 597–603.
7. Yoshida M. Cellular tau pathology and immunohistochemical study of tau isoforms in sporadic tauopathies. *Neuropathology* 2006; **26**: 457–470.
8. Hashimoto N, Takeuchi T, Ishihara R *et al.* Glial fibrillary tangles in diffuse neurofibrillary tangles with calcification. *Acta Neuropathol (Berl)* 2003; **106**: 150–156.
9. Buee L, Delacourte A. Comparative biochemistry of tau in progressive supranuclear palsy, corticobasal degeneration, FTDP-17 and Pick's disease. *Brain Pathol* 1999; **9**: 681–693.
10. Togo T, Akiyama H, Iseki E *et al.* Immunohistochemical study of tau accumulation in early stages of Alzheimer-type neurofibrillary lesions. *Acta Neuropathol (Berl)* 2004; **107**: 504–508.
11. Tanabe Y, Ishizu H, Ishiguro K *et al.* Tau pathology in diffuse neurofibrillary tangles with calcification (DNTC): biochemical and immunohistochemical investigation. *Neuroreport* 2000; **11**: 2473–2477.
12. Yokota O, Terada S, Ishizu·H *et al.* NACP/a-synuclein immunoreactivity in diffuse neurofibrillary tangles with calcification (DNTC). *Acta Neuropathol (Berl)* 2002; **104**: 333–341.
13. Tsuchiya K, Nakayama H, Iritani S *et al.* Distribution of basal ganglia lesions in diffuse neurofibrillary tangles with calcification: a clinicopathological study of five autopsy cases. *Acta Neuropathol (Berl)* 2002; **103**: 555–564.

Original Research Article

Dementia
and Geriatric
Cognitive Disorders

Dement Geriatr Cogn Disord 2009;27:214–223
DOI: 10.1159/000203345

Accepted: October 28, 2008
Published online: February 19, 2009

Neuropathological Investigation of Regions Responsible for Semantic Aphasia in Frontotemporal Lobar Degeneration

Ryoko Yamamoto[a, b] Eizo Iseki[a, b] Shinji Higashi[a] Norio Murayama[a] Michiko Minegishi[a] Kiyoshi Sato[a] Hiroaki Hino[c] Koshiro Fujisawa[c] Kenji Kosaka[c] Takashi Togo[d] Omi Katsuse[d] Hirotake Uchikado[d] Yoshiko Furukawa[d] Mari Yoshida[e] Yoshio Hashizume[e] Heii Arai[b]

[a]PET/CT Dementia Research Center, Juntendo Tokyo Koto Geriatric Medical Center, and [b]Department of Psychiatry, Juntendo University School of Medicine, Tokyo, [c]Hoyu Hospital and [d]Department of Psychiatry, Yokohama City University School of Medicine, Yokohama, and [e]Institute for Medical Science of Aging, Aichi Medical University, Aichi, Japan

Key Words

Semantic aphasia · Frontotemporal lobar degeneration · Semantic dementia · Pick's disease, atypical · Motor neuron disease, dementia with · Ubiquitin · TAR-DNA-binding protein 43

Abstract

Background/Aims: Semantic dementia is a subtype of frontotemporal lobar degeneration, of which an initial symptom is semantic aphasia. Semantic dementia pathologically corresponds to atypical Pick's disease (aPiD), showing ubiquitin-positive inclusions similar to those in dementia with motor neuron disease (D-MND). Previous studies have not clarified the regions responsible for semantic aphasia in aPiD, and there have been no reported neuropathological studies concerning its pathomechanism. ***Methods:*** We neuropathologically investigated aPiD and D-MND cases with and without semantic aphasia. ***Results:*** We determined that the regions involved in the early stage of the disease course of semantic dementia were more restricted to the anterior and inferior portion of the temporal lobe on the side of the dominant hemisphere. ***Conclusion:*** Degeneration of the temporal pole is most likely to participate in the pathomechanism of SA in semantic dementia.

Introduction

Frontotemporal lobar degeneration (FTLD) is characterized by behavior and personality change, language disorder and cognitive decline as well as atrophy of the frontal and anterior temporal lobes. FTLD clinically includes 3 subtypes of frontotemporal dementia (FTD), semantic dementia (SD) and progressive nonfluent aphasia [1]. Each subtype has a characteristic pattern of cerebral atrophy: FTD is associated with bilateral frontal lobe atrophy [2], SD with left-dominant anterior temporal lobe atrophy [3], and nonfluent aphasia with left-dominant perisylvian atrophy [4].

A consensus on clinical diagnostic criteria of FTLD refers to language disorder of SD, including progressive, fluent, empty spontaneous speech, loss of word meaning and comprehension, and semantic paraphasia, which corresponds to semantic aphasia (SA) [1]. Hodges et al. [5] reported 5 cases showing SA in the early stage of the disease course in spite of mild memory problems, when the disease course of FTLD was divided into the early, middle and late stages [1], and defined SD as syndromes presenting with: (1) selective impairment of semantic memory (SA); (2) normal perceptual skills, and (3) relatively preserved day-to-day memory [5].

KARGER

Fax +41 61 306 12 34
E-Mail karger@karger.ch
www.karger.com

1420–8008/09/0273–0214$26.00/0

Accessible online at:
www.karger.com/dem

Ryoko Yamamoto
PET/CT Dementia Research Center, Juntendo Tokyo Koto Geriatric Medical Center
Juntendo University School of Medicine
3-3-20 Shinsuna, Koto-ku, Tokyo 136-0075 (Japan)
Tel. +81 3 5632 3111, Fax +81 3 5632 3728, E-Mail yamamotor@juntendo.gmc.ac.jp

On the other hand, FTD is clinicopathologically classified into the frontal lobe degeneration type, Pick type and motor neuron disease (MND) type. Classical Pick's disease includes 2 clinicopathological subgroups: Pick's disease with Pick bodies showing frontal-dominant lobar atrophy (PiD), and atypical Pick's disease without Pick bodies showing temporal-dominant lobar atrophy (aPiD) [6, 7], although the term of Pick's disease has been recently applied only to cases with Pick bodies. PiD demonstrates tau-positive neuronal inclusions, termed Pick bodies, corresponding to Pick-type FTD [8], whereas aPiD demonstrates ubiquitin-positive, tau-negative neuronal inclusions, corresponding to SD [6, 7]. Similar ubiquitin-positive, tau-negative neuronal inclusions are also found in the MND type of FTD [9], corresponding to dementia with MND (D-MND) [10]. aPiD and D-MND are now included in FTLD with ubiquitin-positive inclusions (FTLD-U) [11], FTLD-U without MND and FTLD-U with MND, respectively, although FTLD-U without MND is not always compatible with SD. The 2 disorders have different appearance patterns of ubiquitin-positive inclusions. Ubiquitin-positive inclusions are found in the frontal and temporal cortices, dentate gyrus and striatum and appear as dystrophic neurites (DNs) in aPiD [6, 12], whereas these inclusions are found in similar regions and appear as neuronal cytoplasmic inclusions (NCIs) in D-MND [1, 9, 13]. TAR-DNA-binding protein 43 (TDP-43) was very recently identified as a major component of ubiquitin-positive inclusions in FTLD-U [14, 15], and DNs or NCIs in both aPiD and D-MND were also positive for TDP-43 [16].

These 2 types of FTLD-U have common clinical features such as personality and social-conduct disorder [1], but different kinds of language disorder: aPiD shows SA and preserved fluent speech in the early stage of the disease course [5, 7, 17], whereas D-MND reveals no SA but altered speech output and dysarthria [10].

Many neuroimaging studies have reported a link between SD and degeneration of the temporal lobe, especially the anterior portion [18, 19]. SD showed focal gray matter tissue loss in the bilateral anterior temporal gyri, amygdala and anterior hippocampal region [2]. Structural image analysis indicated that temporal lobe atrophy in SD includes the parahippocampal, anterior fusiform and middle temporal cortex (MT) [2, 18]. A recent PET study reported that the inferior temporal cortex (IT) showed no activation in SD subjects who had notable deficits in naming despite the normal subjects' activation, while the MT was activated by semantic tasks [20]. Mummery et al. [20] also indicated that the function of the MT is more concerned with semantic knowledge, although that of the IT was concerned with lexical-phonological retrieval. In contrast to these neuroimaging studies, neuropathological studies to examine the regions involved in the early stage of the disease course of SD have not been thoroughly carried out.

In the present study, we neuropathologically investigated 5 aPiD cases with SA and 5 D-MND cases without SA as controls, and attempted to clarify the regions responsible for SA.

Materials and Methods

We examined 10 post-mortem brains from 5 aPiD and 5 D-MND cases. The clinical data of all examined cases are given in table 1, and MRI findings of 2 aPiD cases (in the early stage of the disease course in case 1 and the late stage of the disease course in case 2) are indicated in figure 1. All 5 aPiD cases showed SD in the late stage of the disease course.

Cerebral hemispheres of all examined cases were fixed in 4% paraformaldehyde in 0.1 M phosphate buffer, pH 7.4, embedded in paraffin and cut into 6-μm-thick sections. These cases were pathologically diagnosed with hematoxylin-eosin (HE), Klüver-Barrera (KB), methenamine-silver and Gallyas-Braak methods, as well as immunohistochemical methods described below. Hemispheric serial sections were immunostained with the following antibodies: anti-ubiquitin (ub; MAB1510, monoclonal, mouse, 1:8,000; Chemicon, USA), TDP-43 (polyclonal, rabbit, 1:2,000; Protein-Tech, USA), PHF tau (AT8, monoclonal, mouse, 1:2,000; Innogenetics, Belgium), phosphorylated α-synuclein (Pser129, monoclonal, mouse, 1:20,000, donated by Dr. T. Iwatsubo) [21], amyloid β protein (polyclonal, rabbit, 1:5,000, donated by Dr. T. Ishii), and anti-glial fibrillary acidic protein (GFAP) (polyclonal, rabbit, 1:4,000, Dako, Denmark) antibodies. These sections were pretreated with 70% formic acid for 10 min to TDP-43, phosphorylated α-synuclein and amyloid β protein. Each immunolabel was detected using the avidin-biotinylated horseradish peroxidase complex (ABC) method (Elite Kit, Vector, USA) and visualized with 3,3′-diaminobenzidine tetrahydrochloride (DAB, Wako, Japan).

The degree of neuronal loss with gliosis was evaluated with HE, KB and GFAP stainings in the following regions: frontal cortex (superior frontal, orbital and anterior cingulate cortex), temporal cortex [temporal pole, anterior and posterior portions of the superior temporal cortex (AST and PST), middle temporal cortex (AMT and PMT), inferior temporal cortex (AIT and PIT), entorhinal and parahippocampal cortex], hippocampus (subiculum, CA1 and dentate gyrus) and amygdala, and was graded from 0 to 3, where 0 = absent, 1 = mild neuronal loss with mild gliosis and spongy change, 2 = moderate neuronal loss with moderate gliosis and spongy change, 3 = severe neuronal loss with rare intact neurons, severe gliosis and spongy change. The number of ub-positive inclusions including NCIs and DNs was counted on microscopic fields at ×200 magnification in the same regions. The average number of the largest 3 values of ub-positive NCIs or DNs in each region was calculated separately, and scored from

Table 1. Clinical data of the examined cases

	Age, years	Duration, years	Brain weight, g	Involved lobe	Initial symptoms
aPiD					
Case 1	64	13	810	FL<TL	SA and amnestic aphasia
Case 2	68	4	1,040	FL<TL	SA and amnestic aphasia
Case 3	68	6	1,120	FL<TL	SA and amnestic aphasia
Case 4	70	7	1,095	FL<TL	SA and amnestic aphasia
Case 5	81	5	950	FL<TL	SA and amnestic aphasia
Average	70.2	7.0	1,003		
D-MND					
Case 6	55	4	1,340	FL>TL	weakness of muscle strength and personality change
Case 7	59	3	1,090	FL=TL	weakness of muscle strength and personality change
Case 8	67	3	1,230	FL>TL	weakness of muscle strength and personality change
Case 9	68	4	1,000	FL>TL	weakness of muscle strength and personality change
Case 10	79	6	1,130	FL=TL	weakness of muscle strength and personality change
Average	67.9	5.6	1,215		

aPiD = Atypical Pick's disease; D-MND = dementia with motor neuron disease; FL = frontal lobe; TL = temporal lobe.

(0) to (3), where (0) = absent, (1) = ≥1 but <3, (2) = ≥3 but <9, and (3) = ≥9.

For statistical analysis, SPSS software (v. 14.0) for Windows was employed. The t test was performed for the mean values of grades of neuronal loss or scores of the number of ub-positive inclusions between 2 regions. $p < 0.05$ were considered significant.

Results

The clinical data and brain weights of the examined cases are described in table 1. All aPiD cases showed SA such as difficulty of retrieving the names of objects and semantic paraphasia as well as amnestic aphasia in the early stage of the disease course. Apathy and personality change such as disinhibition and stereotypy followed SA, and then amnesia became apparent. In contrast, all D-MND cases developed weakness of muscle strength of extremities and gait disturbance as well as apathy and personality change in the early stage of the disease course. These cases did not represent SA but altered speech output and dysarthria.

Figure 1a shows the MRI findings of 1 aPiD case (case 1, right-handed) in the early stage of the disease course when SA and amnestic aphasia without dementia were noted. Knife-edged atrophy of the anterior portion of the left temporal lobe was detected. The superior temporal to the fusiform gyrus are also involved, but the parahippocampal gyrus, hippocampus and amygdala are almost preserved. Figure 1b reveals MRI findings of another aPiD case (case 2, left-handed) in the late stage of the disease course when SD was obvious. Knife-edged atrophy of the anterior portion, severe atrophy of the temporal lobe from the superior temporal to the parahippocampal gyrus as well as the hippocampus and amygdala were detected with right predominancy.

Macroscopically, all aPiD cases showed anterior dominant temporal lobar atrophy with unilateral predominancy and relatively preserved frontal lobes (fig. 2a). Severe atrophy of the temporal pole and mild-to-moderate atrophy of the superior temporal to the parahippocampal gyrus as well as the hippocampus were found. On the other hand, all D-MND cases revealed mild atrophy of the dorsal portion of the bilateral frontal lobes with relatively preserved temporal lobes (fig. 2b).

Microscopically, the results of the regional evaluation of neuronal loss in aPiD and D-MND cases are shown in table 2. In aPiD cases, moderate-to-severe neuronal loss was found in the anterior temporal cortex (temporal pole, AST, AMT, AIT and entorhinal cortex), and the average grade ranged from 2.0 to 3.0. The temporal pole showed the most severe neuronal loss, with an average grade of 3.0. The posterior temporal cortex (PST, PMT, PIT and parahippocampal cortex) showed mild-to-moderate neuronal loss that ranged from 1.6 to 2.6. The PIT or parahippocampal cortex showed significantly more severe neuronal loss than PST ($p < 0.05$). The frontal cortex showed milder neuronal loss than the temporal cortex, and this

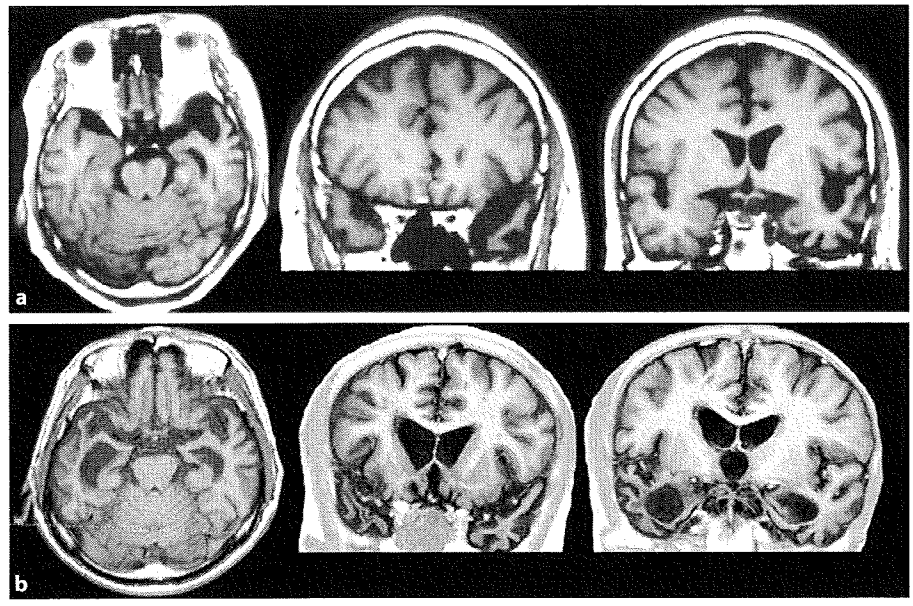

Fig. 1. MRI findings of cases 1 and 2. **a** Case 1 (right-handed) at an early period in the clinical course. The parahippocampal gyrus, hippocampus and amygdala are preserved. **b** Case 2 (left-handed) at late period of the clinical course. Severe atrophy of the temporal lobe from the superior temporal to the parahippocampal gyrus as well as the hippocampus and amygdala, with right predominancy.

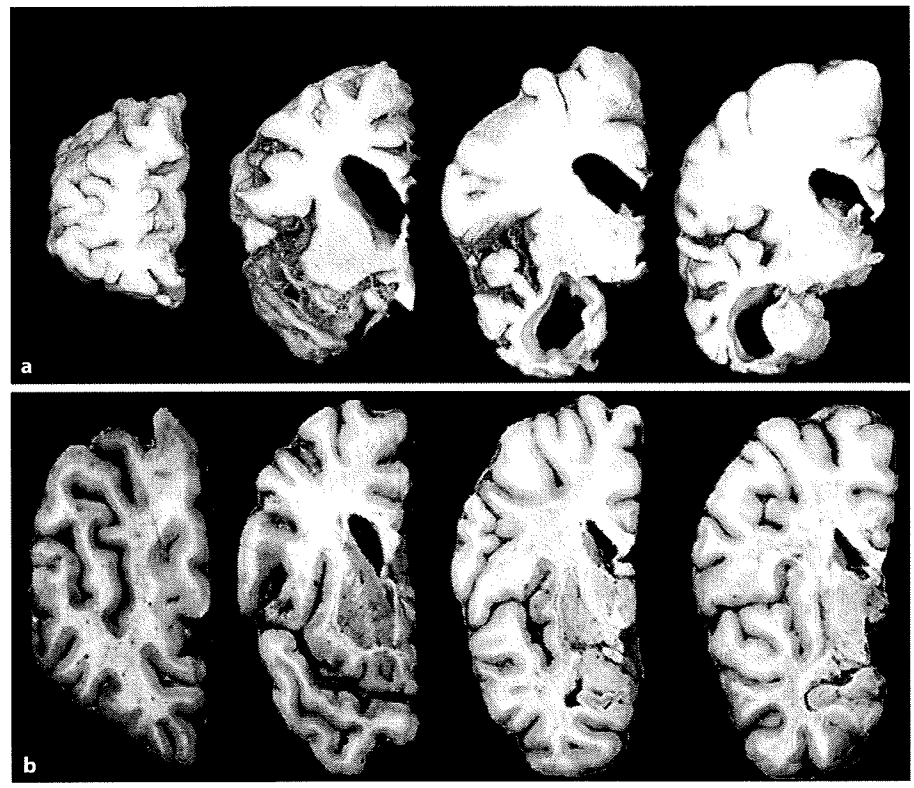

Fig. 2. Macroscopic findings of the cerebral hemispheres of cases 2 and 6. **a** Case 2. Anterior dominant temporal lobar atrophy with right predominancy. **b** Case 6. Mild atrophy of the dorsal portion of the bilateral frontal lobes.

ranged from 1.4 to 1.6. The hippocampus and amygdala showed mild neuronal loss, ranging from 1.0 to 1.5. The temporal cortex showing moderate-to-severe neuronal loss demonstrated neuronal loss and gliosis in the whole layers, especially in layers II–IIIab and V–VI, accompanied by spongy change in layers II–IIIab (fig. 3a, b).

In D-MND cases, both the frontal and temporal cortex showed mild neuronal loss that ranged from 1.2 to 1.6 and from 1.0 to 1.6, respectively. There was no significant difference in neuronal loss between the anterior and posterior temporal cortex. The hippocampus and amygdala showed mild neuronal loss, ranging from 1.0 to 1.5. The